AD NUMBER
AD913412
LIMITATION CHANGES

TO:

Approved for public release; distribution is unlimited.

FROM:

Distribution authorized to U.S. Gov't. agencies only; Test and Evaluation; SEP 1972. Other requests shall be referred to Naval Ship Research and Development Center, Bethesda, MD 20084.

AUTHORITY

NSRDC ltr, 24 Apr 1974

AD 913412

CALIBRATION OF SOME SUBSONIC WIND TUNNEL INSERTS
FOR TWO-DIMENSIONAL AIRFOIL EXPERIMENTS

by

Robert J. Englar
Jonah Ottensoser

Technical Note AL-275

September 1972

NAVAL
SHIP
RESEARCH
AND
DEVELOPMENT
CENTER

BETHESDA
MARYLAND
20034

CALIBRATION OF SOME SUBSONIC WIND TUNNEL INSERTS

FOR TWO-DIMENSIONAL AIRFOIL EXPERIMENTS
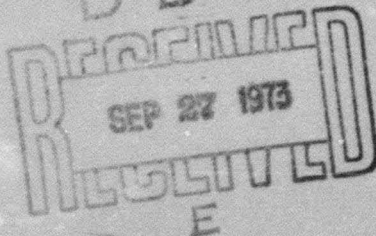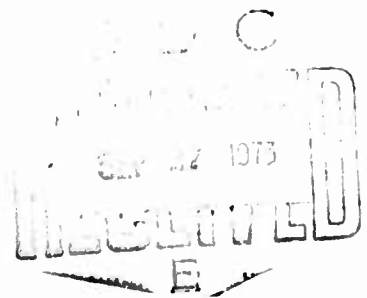

by

Robert J. Englar

Jonah Ottensoser

September 1972   Technical Note AL-275

TABLE OF CONTENTS

LIST OF FIGURES

SYMBOLS

c	model chord, ft
C_a	section axial force coefficient, based on q_∞
C_d	section drag coefficient from momentum loss (wake rake), based on $q_{\infty_{rake}}$
C_ℓ	section lift coefficient, based on q_∞
$C_{\ell_{max}}$	maximum section lift coefficient
$C_{m_{LE}}$	section pitching moment coefficient about leading edge based on q_∞
$C_{m_{25}}$	section quarter-chord pitching moment coefficient, based on q_∞
C_n	section normal force coefficient, based on q_∞
C_p	pressure coefficient, based on q_∞ (or q_{8X10} as noted)
C_Q	pitot-static probe calibration factor
h	tunnel test section height, ft
$\Delta h_{piezometer}$	piezometer pressure differential (total - static pressure), inches alcohol
P_ℓ	local pressure at model or wall taps, lb/ft²
P_{t_r}	total pressure measured by wake rake probes, lb/ft²
$P_{t_\infty}, P_{t_\infty}$	freestream total pressure at the wake rake, lb/ft²
q	dynamic pressure, lb/ft²
q_{OL}	dynamic pressure in outside left channel, lb/ft²
q_{OR}	dynamic pressure in outside right channel, lb/ft²
$q_{probe\ 2}, q_\infty$	dynamic pressure measured by pitot-static probe 2 and corrected using Figure 6, lb/ft²
q_{PZ}	dynamic pressure measured by piezometer ring, lb/ft²

q_{TS} — dynamic pressure in the 3 X 8 ft test section, lb/ft^2

q_∞ — true freestream dynamic pressure (q_{TS} corrected for blockage) lb/ft^2

$q_{\infty_{rake}}$ — freestream dynamic pressure at the wake rake, lb/ft^2

q_{8X10} — dynamic pressure in the 8X10 ft test section, lb/ft^2

R_e — Reynolds number based on chord

V — velocity, ft/sec

V_{10} — velocity at 10th (outermost) probe on boundary layer mouse, ft/sec

x — distance from model leading edge along chord line, ft

X_t — longitudinal distance from tunnel centerline (positive upstream), ft

Y — wake rake probe vertical distance below first tube recorded, ft

Y_{total} — wake rake vertical height, distance from first to last tube recorded, ft

Y_t — lateral distance from tunnel centerline (positive to right), ft

Z_t — vertical distance from tunnel centerline (positive upward), ft

α — local angle of attack, deg.

δ_f — wall trailing edge flap deflection, deg.

ϵ — flow angularity (upwash, positive when flow upward), deg.

σ — flow angularity (sidewash, positive when flow from right), deg.

SUMMARY

Parallel wall inserts were installed in the Naval Ship Research and
Development Center (NSRDC) 8-x 10-foot subsonic tunnel to create a
3-x 8-foot channel to serve as a high flow quality two-dimensional test
section for high lift airfoils. A detailed flow survey indicated good
flow uniformity, negligible angularity, a thin wall boundary layer at the
model station, and a pronounced effect of trailing edge wall flaps on
controlling test section dynamic pressure. Airfoil data obtained in the
facility displayed good agreement with reference data in lift and pressure
distribution, but some disagreement in wake rake drag data. The strong
influence of model lift on test section dynamic pressure measurement was
noted, and a measurement technique was developed which was independent of
the static pressure field propagating from the airfoil.

INTRODUCTION

In conducting two-dimensional testing of high lift blown airfoils for both fixed and rotary wing application, the requirement arises for a subsonic facility specifically configured to minimize the particular problems of this type of testing. As discussed in Reference 1, these problems are primarily associated with the interaction between the high lift model pressure distribution and the limiting physical features of the test section. In addition to increased flow blockage, a small tunnel-height-to-model-chord ratio can yield induced camber (lift interference) effects on the model measured forces which can be difficult to correct. Close proximity of the blown model to the floor can invalidate test results due to impingement of the jet wake on that boundary. The primary problem resulting from high lift pressure fields is their reaction with the test section wall boundary layer, which can produce separation of the wall boundary layer and such severe three-dimensional effects that the data is frequently invalidated.

In the absence of a tunnel specifically designed for two-dimensional work, the most effective alternative has been to divide an existing subsonic test section into three channels by the installation of vertical wall inserts spanning the original test section from floor to ceiling. If properly designed, this setup will provide a high quality two-dimensional test facility by: (1) greatly reducing the wall boundary layer thickness since its development is only from the leading edge of the inserts and not from far upstream in the settling chamber; (2) providing reduced structural loads on the model since it only spans a reduced width test section; (3) and allowing a larger height-to-chord ratio, since the chord on the reduced span model is usually not as large as a full span model. An additional benefit is an increase in the maximum available test section dynamic pressure. The one major difficulty encountered with this arrangement is the determination of the effective freestream dynamic pressure, since flow conditions in the test section and two outside channels are not alike (due to model blockage and upstream propagation of lift disturbances). A careful calibration of

the tunnel under known flow conditions is thus required before meaningful airfoil test data can be obtained.

A two-dimensional facility of the type just described was constructed and installed in the 8- x 10-foot subsonic South Tunnel at the Naval Ship Research and Development Center (NSRDC). The following is a detailed discussion of the design and calibration of the facility and results of two tests conducted on reference 2-D airfoils to ascertain the quality of data produced.

DESIGN CONSIDERATIONS

The two-dimensional test facility was to be non-permanent and easily installed within the 8- x 10-foot test section. Structurally, the insert walls were required to withstand the high aerodynamic loads imposed by a section lift coefficient of 8 at dynamic pressure of 70 lb/ft^2 over an airfoil section of 6 ft^2 planform area. Trailing edge flaps on the walls were intended for balance of flow between the test section and outside channels, while the leading edges of the walls were to produce smooth, uniform, unseparated flow at the entrance into the test section. Control of the wall boundary layer was to be accomplished by use of tangential blowing slots located in the walls upstream of the model and on the mounting turntable in the vicinity of expected adverse pressure gradients on the model. In view of the preference for force and moment data obtained from pressure instrumentation (Reference 1), surface pressure taps and a wake rake were to be employed. This would eliminate complex balance mechanisms in the walls as well as the inaccuracies caused by balance tares and induced flow angularity. Two-dimensionality would be monitored by spanwise static taps on the model and by flow visualization, for which transparent end plates and windows in the walls would be provided.

FACILITY DETAILS

Taking into account the design and construction of similar facilities described in References 2 and 3, the NSRDC two-dimensional wall inserts

2

were designed and constructed as shown in Figure 1. The walls were 4 inches thick, with a main structure of I-beams covered with 3/8" plywood. The 1" thick turntable model mounts, one of which was plexiglass, were mounted in steel plates attached to the I-beam framework, and could rotate ±20 degrees. Trailing edge flaps of 38-inch chord were able to deflect ±20 degrees, and formed a flush straight continuation of the test section when deflected inward to -2.58 degrees. The overall wall length of 175 inches extended 5 inches beyond the downstream limit of the parallel floor and ceiling of the original test section. The contoured leading edges of the walls were 7.41 inches in length, and designed to prevent flow separation. Based on design criteria for circular propeller shroud inlets (Reference 4), the inside profile of the leading edge was elliptic, fairing into a smaller radius circular cylinder on the outside of the wall. These were pressure tapped to monitor inflow conditions. For the initial flow calibrations and tests of the two relatively low lift reference airfoils, no wall boundary layer separation was anticipated, and thus the wall tangential blowing slots were not incorporated.

EMPTY TEST SECTION CALIBRATION

Calibration of the 3-x 8-foot test section channel was carried out over a range of velocity settings and flap deflections with no model present to determine the following:

1. Correlation of true dynamic pressure in the test section with some reliable reference measurement which would not be affected by model lift.

2. Uniformity of the flow (dynamic pressure, angularity) in the vicinity of the model location.

3. Wall boundary layer characteristics at the model location.

4. Effect of flaps on flow distribution through the three channels, and on flow uniformity in the test section.

5. Inflow conditions at the wall leading edges.

3

The following instrumentation was arranged as shown in Figures 1, 2, and 3 to record the above data:

1. Five pitot-static probes, positioned as follows (looking upstream)

    Probe 1:   horizontal centerline of test section floor

    2:   vertical centerline of test section right wall, in test section

    3:   vertical centerline of test section right wall, outside channel

    4:   vertical centerline of test section left wall, outside channel

    5:   horizontal centerline of test section ceiling

    Probes 1 through 4 were located 32 inches downstream of the wall leading edge (or 24.59 inches from beginning of the flat wall) while probe 5 (the original probe for the 8-x 10-foot section) was approximately one inch downstream of the leading edge.

2. A 12 probe pitot-static yaw head rake.

3. A boundary layer mouse with 10 total head and 4 static probes, located at a measuring station on the vertical centerline of the left wall, and 12 inches upstream of the test section center, which corresponds to the leading edge position of a two-foot chord model.

4. Static pressure taps in the wall leading edges (11 in the right wall and 6 in the left) located on the vertical centerline and spaced as in Figure 15.

5. A piezometer ring in the entrance to the 8-x 10-foot test section for determination of dynamic pressure in the original facility.

6. A total temperature thermocouple in the settling chamber.

Initial calibration of the empty test section was conducted using all the above instrumentation with the exception of the yaw head rake, which was expected to produce some slight blockage effects. For constant values of trailing edge flap deflection, varying values of dynamic pressure were set using the piezometer ring to adjust flow velocity into the 8-x 10-foot section, and dynamic pressures in the three channels were recorded. Figure 4 presents the correlation factor between the dynamic pressure set on the piezometer ring (q_{PZ}, as indicated by the

4

pressure differential $\Delta h_{piezometer}$) and the true dynamic pressure in the 8-x 10-foot test section without the insert walls. This factor accounts for the piezometer ring location in the entrance rather than in the parallel wall test section and for the variation at low Reynolds number ($\Delta h_{piezometer} \leq 8$ in. alch). The variation of dynamic pressure in the 3-x 8-ft insert test section as a function of both flap setting and q set using the piezometer ring (q_{PZ}) is shown in Figure 5. The actual test section dynamic pressure (q_{TS}) was measured with pitot-static probe 2 (see Figure 1) and was corrected in accordance with the calibration in Figure 6. Additional data was taken with a single pitot-static yaw head probe and are represented by the flagged symbols in Figure 5. The ratio q_{PZ}/q_{TS} is presented because it relates dynamic pressure in the inserts to q indicated on the piezometer ring, which is the quantity monitored by the tunnel operator. As Figure 5 shows, flap deflection is very effective in increasing the test section q, which can be as much as double the value in the 8-x 10-foot test section for the same piezometer setting ($\Delta h_{piezometer}$). The maximum tunnel q of approximately 65 lb/ft^3 for the original facility can be increased to over 100 lb/ft^3. The maximum flap effectiveness ($\Delta q/\Delta \delta_f$) occurs for the smaller deflection angles; at higher angles the flaps begin to block the flow through the outer channels (38 inches wide), and a maximum q through the test section is reached. Upon examination of the flow through the outer channels, it was found that the dynamic pressures in the two channels were not the same. Figure 7 depicts this inequality, where the flow through the left outside channel is greater than through the right for all flap settings.

Based on problems experienced in other facilities of this type, it was anticipated that with a lifting model in the test section, pressure disturbances were likely to propagate forward to probe 2, which had been used to determine freestream dynamic pressure in the empty test section. As this was likely to yield appreciable error in freestream dynamic pressure, it was desired to have a reliable indicator of freestream q which would not be affected by model presence. It was reasoned that an accurate determination of q in the outside channels should be free of model lift effects, and that test section q could be determined from continuity of mass flow through the entire test area. To this end,

5

Figures 8 and 9 were plotted from empty test section data as calibration curves, where the test section dynamic pressure could then be determined based on left or right channel flow. These values were nondimensionalized by piezometer q, indicative of total mass flow into the three channels before splitting, and thus causing curves for varying $\Delta h_{piezometer}$ to collapse into essentially one curve. In this calibration, the function of the flap deflection is to simulate model blockage (or lack of) so that varying flow rates are produced in the outside channels. It was thus intended that with a high lift model in place, the test section dynamic pressure could be calculated from a curve fit of Figures 8 or 9 when only q_{PZ} and q_{OL} or q_{OR} were measured.

Typical velocity profiles in the wall boundary layer 12 inches upstream of the vertical centerline are shown in Figure 10 for flap angles of $-2.58°$ and $20°$, and for three dynamic pressures. Very little difference due to flap angle or dynamic pressure variation is noted. The outer edge velocity returned to freestream value at about 1 inch distance from the wall; for the original 8-x 10-foot tunnel with boundary layer developing upstream in the settling chamber, this distance was on the order of 2 to 3 inches. This reduction due to the shorter length of the insert walls should substantially reduce the boundary layer problem at high lift, while decreasing the mass flow requirements for any blown-or suction-type boundary layer control system employed to eliminate the velocity deficit.

Figure 11 displays the Reynolds number range available for the range of test section dynamic pressures of Figure 5. Reynolds number of 1.8 million per foot, or roughly 3.6 million for a 2 foot chord airfoil section, was generated in the empty test section. It is to be expected that this number will be reduced due to blockage when an actual airfoil is installed.

A second phase of the empty test section calibration involved determining the flow quality in the test region; i.e., q deviation from a reference value, and flow angularity. The pitot-static yaw probe rake of Figure 3 was installed at the longitudinal and vertical centerline; and later at stations 9 inches above and below the vertical centerline. The rake employed 12 probes, 1 inch apart, with one extreme 6.5 inches from

6

the tunnel wall, and the other 1/2 inch from the tunnel centerline.
Each probe was 10 inches in length and had a 0.134 inch diameter hemi-
spherical head with a total head pickup at the center and 4 static taps
located on the curved surface of the head at $90°$ radial spacing. An
additional tap to measure freestream static pressure was located 0.895
inches downstream of the tip of each probe. A sample distribution of
upwash (ϵ), sidewash (σ) and dynamic pressure deviation ($\Delta q/q_{TS}$) is
shown in Figure 12, taken on the vertical and longitudinal centerlines
and spanning the left half of the test sect.on channel. As there is
some scatter in the data, they were averaged across the span of the rake
to enable better interpretation. Figure 13 presents the average dynamic
pressure deviations using probe 2 as reference; the band of data shown
indicates average variations of ±2 percent over the entire q range. This
error may be slightly high in that the reference probe is located 46.6
inches upstream of the rake, and a small q deviation in the longitudinal
direction may exist.

Figure 14 presents the averaged values of upwash and sidewash of the
flow. Whereas the sidewash angle is relatively low and varies slightly
with flap angle, it is seen that upwash varies between 0.50 and 0.90
degrees, increasing with q and decreasing with flap angle. Careful ex-
amination of alignment of the rake probes revealed that some slight
vertical bending of the probes occurred under the weight of the setting
inclinometer. With the angle zeroed and the weight removed, the tubes
apparently sprang to a slightly positive angle. Furthermore, it appears
that additional upward bending occurred as increased lift developed on
the inclined probes as q was increased. The conclusion that the upwash
was somewhat less than indicated was later verified by comparing airfoil
data at the same angle as data for the airfoil inverted.

Pressure distributions on the wall leading edges are shown in
Figures 15 and 16. Reynolds number variation has little effect on the
inside wall distribution and on the stagnation point, but increased R_e
on the sharp outside radius produces an increasing suction peak followed
by a strong adverse pressure gradient which might well have led to flow
separation. For increased flap deflection (more flow into the test

7

section) the Reynolds number effect became less noticeable. In these C_p distributions, the reference static and dynamic pressures are taken as those in the 8- x 10- foot test section as derived from the piezometer ring and Figure 4; that these are proper values is verified by $C_p = 1.0$ being calculated at the stagnation point. At constant Reynolds number, Figure 16 shows the effect of flap deflection on the leading edge pressures. With increase in flap setting, the stagnation point moves from in the test section to the outside channel side of the wall. A large suction area forms over the inside wall, yet the wall shape is such that no sharp peaks form, and no severe adverse gradients are present - separation apparently is not a danger for the range of flap deflections available.

DYNAMIC PRESSURE DETERMINATION IN PRESENCE OF MODEL

A difficult problem which frequently has occurred in test facilities of this type has been the determination of true freestream dynamic pressure (q_∞) in the center test section. As the amount of mass flow through the test section varies with model blockage and lift (or with flap deflection) normal methods of q determination are often invalid. Frequently, due to the limited wall length, the freestream static pressure reference tap cannot be located far enough upstream to be unaffected by the high lift pressure field (see Reference 5) and yet also be far enough downstream as to be free of the wall leading edge influence. For these reasons, it becomes necessary to determine q_∞ from some means which is independent of model lift and blockage. During the empty test section calibration, pitot-static probe 2 was used to determine actual test section dynamic pressure, while the dynamic pressures in the outside two channels and into the total 8- x 10- foot test section were recorded by probes 3 and 4 and the piezometer ring. Using the values recorded by tubes 3 and 4 and the piezometer ring in conjunction with the continuity of mass flow through the system, an accurate determination of dynamic pressure in the 3- x 8- foot test section was obtained. Based on the physical dimensions of the facility and assuming no wall boundary layer displacement thickness, the continuity equations yields:

8

$$q_{TS} = [3.3333 \ (q_{8x10})^{\frac{1}{2}} - 1.0567 \ (q_{OR}^{\frac{1}{2}} + q_{OL}^{\frac{1}{2}})]^2 \tag{1}$$

where q_{8x10} is between the parallel walls of the 8 x 10 test section, obtained from the piezometer ring and Figure 4. It was found that q_{TS} determined in this manner agreed very well with the measured data of Figures 8 and 9. It was initially decided to mathematically curve fit the empty test section data of Figure 8 or 9, input a measured value of q_{OR} or q_{OL} from the outside channel, and calculate the test section q from the curve fit. Attempts at this procedure showed, however, a significant error of 5-6% or more in q_{TS}; the single faired curve apparently did not accurately represent all the data of Figures 8 and 9. When the continuity equation was used instead, agreement with the measured q_{TS} was considerably improved - this technique took into account those points which were somewhat displaced from the curve fit and had thus been inaccurately calculated by that method. As the agreement held accurately with flap deflections from -2.58° to 20°, thus simulating variations in mass flow through the center test section, it was decided to use the continuity calculation of dynamic pressure for conditions with blockage and lift.

REFERENCE AIRFOIL TESTS

Two pressure tapped reference airfoil sections of 3 foot span were available for use: a 20-inch chord NACA 65-213 (a = 0.5) on loan from Grumman Aerospace, intended as a 2-D calibration airfoil; and a 23-inch reference 2-D section from NASA, Langley Research Center, which had previously been thoroughly tested in subsonic flow in their 3-ft span 2-D tunnel (not a wall insert setup). The 65-213 is shown installed in the NSRDC 3-x 8-ft inserts in Figures 17 and 18. Probe 2 has now been moved 10.5 inches forward of its original position and 2 feet upwards in an attempt to minimize influence from the model. A 110 tube wake rake was located 42 inches downstream of the centerline (roughly 1.33 to 1.60 chords from the model trailing edge, depending on which model was used), with 42 total tubes and 5 static probes in the vicinity of the model being

recorded by a multiple scannivalve pressure readout employing a ±1.0 psid
Statham transducer. As high lift was not anticipated for either model,
wall boundary layer control was not incorporated (it had not been used
for the reference data either). However, both models had spanwise
pressure taps on the upper surface in at least 2 chordwise stations to
monitor lateral uniformity. No strong three-dimensionality was observed
by these taps during the tests, with the exception of several cases
beyond the stall incidence.

NACA 65-213 (a = 0.5)

The 65-213 section was run over an angle of attack range from
-4° to +16° and dynamic pressure from 10 to 80 lb/ft² (R_e = .9 x 10⁶ to
2.6 x 10⁶). To produce this range of tunnel velocity, the wall flaps
were set at 5° throughout the test - no adjustment was needed to allieviate
blockage. Tunnel dynamic pressure determined from continuity as discussed
above was corrected for solid blockage only; then lift and pitching moment
(both from pressure integration) and angle of attack were corrected as
follows for lift interference and camber effect (see References 1 and 6)
for c/h = .208

$$\Delta C_\ell = - \frac{\pi^2}{48} \left(\frac{c}{h}\right)^2 C_{\ell_u} = -.008924 \, C_{\ell_u} \tag{2}$$

$$\Delta C_{m_{25}} = \frac{\pi^2}{192} \left(\frac{c}{h}\right)^2 C_{\ell_u} = .002231 \, C_{\ell_u} \tag{3}$$

$$\Delta \alpha = \frac{57.3\pi}{96} \left(\frac{c}{h}\right)^2 [C_{\ell_u} + 4C_{m_{25_u}}] = .081386 \, [C_{\ell_u} + 4C_{m_{25_u}}] \tag{4}$$

where subscript u indicates the uncorrected value. Figure 19 presents
section lift and moment coefficients as functions of incidence for constant
values of dynamic pressure. The Reynolds number effect on $C_{\ell_{max}}$ is quite
apparent. Figure 20 presents pressure distributions for a range of
Reynolds number at α = 13°, just before stall, while Figure 21 shows a
similar effect at other incidences. For comparative purposes, data from

10

Reference 7 for a NACA 65-212 (a = 0.6) at R_e = 3 x 10⁶ are shown as the dashed curves in Figure 19. The agreement with the present lift data is good; the additional $C_{\ell_{max}}$ for the 65-212 is easily attributable to the increased test Reynolds numbers of that airfoil. The same is true for the difference in stall incidence. The cause for the discrepancy in quarter-chord pitching moment coefficient is not immediately apparent without pressure distributions for the 65-212 section. The distributions for the present airfoil are presented in Figure 22 at constant q and over a range of incidence. An interesting feature occurs at $\alpha = 12.1^{\circ}$ degrees, where a small leading edge separation forms, accompanied by a loss in lift, but then disappears at $\alpha = 13^{\circ}$. Complete stall immediately follows.

An estimate of the effect of these relatively low lift coefficients on pitot-static probe 2 is shown in Figure 23 for two values of dynamic pressure. The upper surface static pressure field at $C_{\ell} \approx 1.3$ can apparently create as much as a 6 to 9 percent increase in $q_{probe\ 2}$ over the zero lift value. One might expect that probe 2 may also be influenced by a static pressure drop (greater suction) in the vicinity of the wall leading edge caused by increase in q, as the upper curve in Figure 23 has increased by roughly 7 percent at C_{ℓ} = 0 when the dynamic pressure is approximately doubled. The probe's new location 10.5 inches ahead of the empty test section position may have added to its sensitivity to the wall leading edge pressure field, but likewise should have reduced influence from the model. It should be noted that in Figure 23 (as well as Figures 34 and 35), the ratio's denominator is freestream dynamic pressure determined from continuity and corrected for blockage.

Figure 24 presents the 65-213 drag polar for two dynamic pressures, where it is seen that outside of the drag bucket or minimum drag range, agreement between the 65-213 at R_e = 2.3 x 10⁶ and 65-212 at R_e = 3 x 10⁶ is excellent. However, for the few points within the minimum drag range, measured drag is quite high. As test emphasis was on lift results near stall incidence, very few points were taken in the linear portion of the lift curve, and thus an insufficient amount of drag data is present to draw any firm conclusions at low lift. The faired curves approach the

11

shape of the standard roughness curve for the 65-212 airfoil, hinting that there may have been some surface roughness effect on the test airfoil. One additional possibility is that the drag rake, located 18 inches upstream of the wall flap knee, may have been influenced by the static pressure field from the flap at 5 degrees. Sample total pressure distributions from the rake are presented in Figure 25 for $q_\infty \approx 66$ lb/ft². The downward wake movement relative to the model on the tunnel centerline indicates the increased wake deflection with lift, while stall suddenly brings on a large total pressure deficit over the upper wake and little change relative to the lower surface.

NASA REFERENCE SECTION

A characteristic reference airfoil section was tested at subsonic speeds ($q_\infty \approx 30$ psf, $R_e \approx 2 \times 10^6$) by NASA, Langley Research Center, and conveniently was the proper span for installation between the NSRDC 2-D inserts. The airfoil was of solid aluminum with a 23-inch chord and a very smooth finish except at the center span. Here, a grove had been machined, pressure tubing laid in and drilled, and a plastic-like resin applied over the tubing to reform the original surface. However, the resin felt very rough to the touch, and since this was in the immediate location of the pressure taps by which all lift and moment data was determined, it is surmised that this data thus reflects some, if not considerable, roughness effect. Tests were conducted over an incidence range of $-4° \leq \alpha \leq 18°$, and freestream dynamic pressures of roughly 10, 32, and 66 lb/ft² ($R_e = 1.07 \times 10^6$, 1.92×10^6, and 2.74×10^6). Corrections to the data for induced camber effect based on c/h = .240 were as follows.

$$\Delta C_\ell = -.011802\ C_{\ell_u} \tag{5}$$

$$\Delta C_{m_{25}} = .002951\ C_{\ell_u} \tag{6}$$

12

$$\Delta\alpha = .107633 \left[C_{\ell_u} + {}^{4}C_{m_{25_u}} \right] \tag{7}$$

Test section q was determined from continuity considerations as before, and corrected for solid blockage; a constant wall flap setting of 5° was maintained, and no wall boundary layer control was employed. The model was tested both in the normal upright position, and in an inverted position, primarily to evaluate flow angularity which was in doubt due to possible misalignment of the yaw head survey rake.

Figure 26 presents normal force coefficient (which avoids the angle-dependent resolution of normal and axial forces into lift) as a function of incidence for NSRDC and NASA data at $q_{\infty} \approx 32$ lb/ft^2. The agreement is excellent, relative to Langley data, with the exception of two points at stall or beyond. Very close repetition of the NSRDC upright data by the inverted data indicates that flow angularity, if existent, is not discernable, and will therefore be assumed negligible. This confirms the previous hypothesis that the indicated flow upwash was caused by yaw probe misalignment and resultant normal force loading. Figures 27 and 28 present the effect of Reynolds number on both the upright and inverted airfoil lift curves, where both $C_{\ell_{max}}$ and α_{stall} increase with higher R_e. Agreement between upright and inverted data is good with the exception of the $q_{\infty} = 32$ lb/ft^2 curve, where stall occurs 2° earlier for the inverted case. Corresponding pressure distributions for these Reynolds numbers at $\alpha = 16^{\circ}$ are shown in Figures 29 (upright) and 30 (inverted). The stalled pressure distribution of the inverted section is clear, as is the unstalled condition of the upright airfoil at the same incidence. A possible explanation is that of a slight discrepancy in incidence in the immediate vicinity of stall, causing the onset of separation in the inverted case only. Otherwise, the $q_{\infty} \approx 10$ and 70 lb/ft^2 distributions in Figures 29 and 30 are practically identical to their respective inverted cases.

Further insight into the lift properties of the NASA reference airfoil is provided by the pressure distributions at three selected angles of attack, Figures 31-33.

13

The effect of the model static pressure field on dynamic pressure measured by probe 2 is seen in Figures 34 and 35. For the upright model (Figure 34) the same increase in indicated q with C_ℓ is found as in Figure 23: roughly a 6 to 10 percent increase from the $C_\ell = 0$ case is found at $C_\ell = 1.6$, and again an increase at $C_\ell = 0$ of about 6% is produced by doubling the dynamic pressure. Because probe 2 was located 2 ft above the tunnel centerline, inversion of the model considerably removes the measuring location from the upper surface suction region, and q_2 thus converges towards true test section q as lift increases. (Figure 35). A 2.1% discrepancy at $C_\ell = 0$ still remains, suggesting that the upper surface suction is probably not responsible for the zero-lift shift. Figure 35 also shows (for one C_ℓ only) the effect of flap defelction on the indicated q_2, another justification of the need for determining dynamic pressure by an alternate means.

Quarter-chord pitching moment coefficient as a function of normal force and incidence was presented in Figure 26, where agreement with NASA data was relatively good except at stall. The NASA data, in general, shows a slightly larger nose-down pitching moment; the same trend is true in Figure 36, where leading edge pitching moment is plotted against normal force coefficient.

The usual error in axial force coefficient resulting from inaccurate measurements of the pressure tap vertical location is still existent in the data of Figure 37, but since the actual measurements used were those supplied by NASA, the agreement between the two tests is relatively good. Discrepancy is possibly caused by NSRDC use of a simple trapezoidal rule summation of the incremental axial pressure forces, rather than a more sophisticated one used by NASA. However, all other NSRDC lift, drag and normal force data were integrated using a modified Simpson routine of much greater accuracy than the trapezoidal rule. This Simpson routine was also used in a sample case to integrate NASA C_p data and gave exactly the same normal force value, indicating the equivalence of these two numerical routines. The trapezoidal rule was used in the moment data of Figures 26 and 36, and may be responsible for the discrepancy there as well. The drag polars for upright, inverted and NASA data are compared

in Figure 38 for q_∞ = 32 lb/ft². Above C_l = 0.6, the NASA data falls
between the upright and inverted data, while in the minimum drag region
of NSRDC data, NASA data rises rather rapidly with decreasing C_l. The
cause of the non-agreement between upright and inverted curves is not
readily apparent. The momentum deficit was read on different portions
of the wake rake with different tube spacing for the two curves, and
there was a difference of as much as 10 percent in corrected q between
upright and inverted. Related to the later point was a difference in
the static pressure gradients from floor to ceiling for the two cases.
A combination of these may be responsible for the differences of Figure 38;
based on the NASA data, the correct result should lie between the two
curves. Figures 39 and 40 depict Reynolds number effect on the drag polars,
which is a decrease in drag coefficient with increased R_e, except in the
minimum drag regime. There the opposite is true, with some rise in drag
due to greater Reynolds number. This same trend was displayed by the
65-213 in Figure 24.

Total pressure distributions in the rake for variation in Reynolds
number at α = 16° are presented in Figures 41 and 42; and give an insight
into the drag rise in Figures 39 and 40. Figure 43 presents variation
in the measured momentum deficit with angle of attack at fixed Reynolds
number.

As mentioned earlier, it is felt that some influence from the trailing
edge wall flaps may have been felt by the wake rake. In addition, the
rake static pressure probes indicated a gradient from ceiling to floor.
It would have been desirable to calibrate the empty test section with the
wake rake in place, both to examine vertical static pressure gradients
and to investigate the effect of flap deflection on the static pressure.
It is recommended that this be done before further testing is undertaken,
as there is a possibility that the present rake location is non-optimum.

OPERATING PROCEDURE

As previously emphasized, the primary difficulty in operation of a
tunnel which has been converted to a two-dimensional insert facility

composed of three separate channels is the correct determination of dynamic pressure in the test section (q_{TS}) so that tunnel power may be set accordingly. This problem arises from the influence of the static pressure field on a lifting model (and to a lesser extent the pressure field from the leading edge of the insert walls) on the pitot-static probe mounted within the test section which would ordinarily be used to set dynamic pressure. This unfavorable effect has been shown in Figures 23, 34, and 35. It should be stongly noted, however, that while a particular desired value of test section dynamic pressure is difficult to accurately set, one the tunnel conditions are established (i.e., power and flaps set), the existing dynamic pressure may quite accurately be determined using equation (1). It is thus not a problem to determine the test section dynamic pressure within the inserts, but rather to be able to physically set a desired value. Unless severe Reynolds number effects on lift and drag coefficient are present over a small range of dynamic pressures, then this missetting of q_{TS} to within a few percent should pose little problem.

For the reference airfoil tests conducted in which the model was inverted and the pitot-static probe was thus beneath the lower surface of the airfoil section, the probe was least affected. If dynamic pressure values on the order of 6 percent deviation or less from a desired q_{TS} can be tolerated, the pitot-static probe can be used within the test section to set q_{TS} and should be placed beneath the model lower surface. This is perhaps the simplest method of setting tunnel power and could suffice in many cases. In addition, this 6 percent deviation can be reduced by generating curves similar to Figure 35 from a few preliminary runs and using them to estimate the value of $q_{probe\ 2}$ necessary to set a desired freestream dynamic pressure (which when reduced by the solid blockage correction is merely q_{TS}). As C_ℓ increases, the necessary compensation decreases, at least until the range of Figure 35 data is exceeded. Figure 23, 34, and 35 are, of course, distinct for the specific airfoils tested, and should be similar in shape but not magnitude to other airfoil sections.

A more exact method of setting test section dynamic pressure is as follows, but is somewhat more complex than the above:

1. Choose the desired freestream dynamic pressure (q_∞) and reduce it by the solid blockage factor to obtain q_{TS}.

2. Set flap angle, δ_f, and refer to Figure 7 to relate q_{OL} to q_{OR} and to q_{TS} for that flap setting. For example, for $\delta_f = 10°$ and $q_{TS} = 30$ psf, then $q_{OR} = 13.5$ psf and $q_{OL} \approx 1.06\ q_{OR}$. Use this relationship to eliminate q_{OL} (or q_{OR}) from equation (1).

3. Solve Equation (1) for q_{8X10}, then use Figure 4 to determine piezometer ring setting. Set tunnel power accordingly.

4. Monitor q_{OR} (or q_{OL}) for the value determined in Step 2. Some slight adjustment of the flaps may be necessary before the proper value of q_{OR} is reached, since Figure 7 results are for the empty test section, and will be somewhat different with an airfoil installed in the middle channel.

This method eliminates use of probe 2 altogether and thus is not affected by model influence. An alternative to flap adjustment is to fix flap angle and adjust tunnel power (and thus q_{8X10}) while monitoring q_{OR}. This eliminates a second tunnel operator required to control the flaps, but requires that Equation (1) be resolved whenever q_{8X10} is changed. In either case, adjustments of some type will most likely have to be made to obtain the desired values of q_{OR} and thus q_{TS}. From the standpoint of simplicity, it appears that perhaps the first method (use of probe 2 below the airfoil and preliminary curves similar to Figure 35) is to be preferred, since the deviation from desired test section dynamic pressure can probably be held to a few percent, and determination of the actual value can be made regardless of the method used to set it.

CONCLUSIONS

A set of parallel wall inserts was installed in the NSRDC 8- x 10-foot subsonic tunnel to create a high height-to-chord ratio facility with reduced wall effect for use in high lift testing. A detailed flow survey indicated high flow uniformity, negligible flow angularity in upwash, a 1-inch thick (or less) wall boundary layer, and a strong effect of trailing edge flaps on control of test section dynamic pressure (including

17

an increase of over 60% in test section maximum). Two reference airfoil sections tested in the facility indicated the adverse effects of model pressure field on determination of true freestream dynamic pressure, making necessary the use of an alternate method accounting for continuity of mass through the three channels. With the proper dynamic pressures employed, lift and pressure distribution data agreed well with that available for the reference sections. Difficulty in accurate measurement of section drag, even employing the wake rake momentum loss technique, caused comparison of drag data to be somewhat less in agreement. This may have been due in part to some lack of accuracy in the reference data as well. Additional investigation should be conducted into factors influencing the rake before additional testing is begun. Furthermore, tangential wall blowing slots need to be installed to control the wall boundary layer for future high lift tests, and an evaluation of their installed effectiveness made. Otherwise, agreement was sufficiently good to confirm the wall inserts as an adequate facility for quality two-dimensional testing.

ACKNOWLEDGEMENT

REFERENCES

1. Englar, R. J. and R. M. Williams, "Test Techniques for High Lift Two-Dimensional Airfoils with Boundary Layer and Circulation Control for Application to Rotary Wing Aircraft", Canadian Aeronautics and Space Journal, Vol. 19, No. 3, pp 93-108, Mar 1973.

2. McDonnell Aircraft Corporation, Report No. G 369, pp 211-222.

3. General Dynamics, Convair Division, Report ZT-043, pp I-6.200 to I-6.210.

4. Johnson, Arthur E. and William B. Maguire, "Static Tests of Ten Related Circular Shroud Inlets", Washington, Mar 1966 (Naval Ship Research and Development Center Report 2171, Aero Report 1104).

5. Woodward, D. S., "On the Errors Induced at Tunnel Reference Pressure Tappings by High Lift Models", Feb 1966 (RAE TR 66049).

6. Carner, H. C., E. W. E. Rogers, et. al., "Subsonic Wind Tunnel Wall Corrections", Paris, Oct 1966 (AGARDOGRAPH 109).

7. Abbott, Ira H. and Albert E. Von Doenhoff, Theory of Wing Sections. N.Y., Dover Publications, Inc., 1959.

Figure 1 - Facility Layout and Geometry
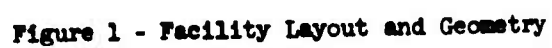
Figure 2 - Two-Dimensional Inserts Installed in 8 x 10 Ft. Subsonic Tunnel
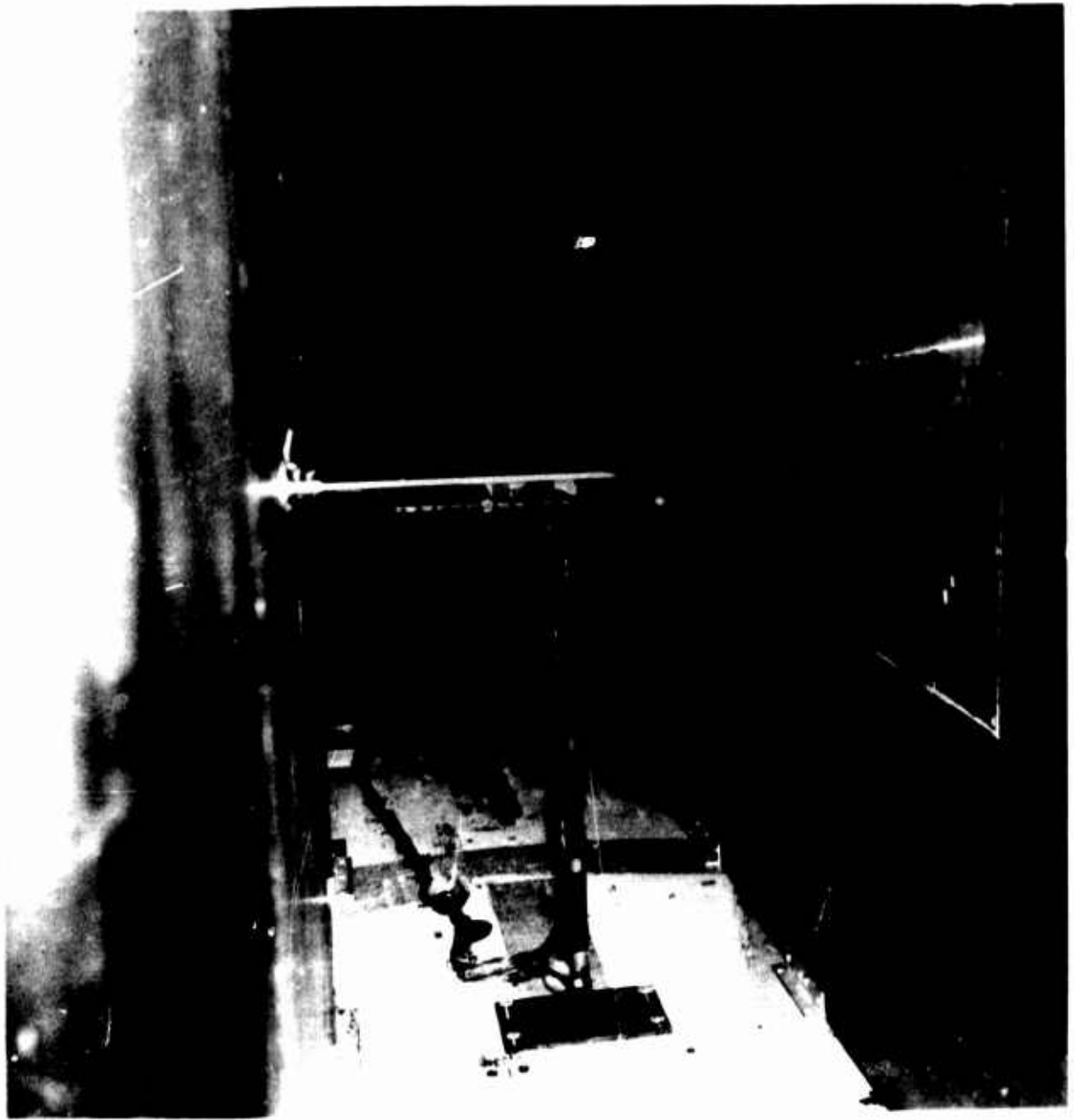
Figure 3 - Empty Test Section Calibration Instrumentation
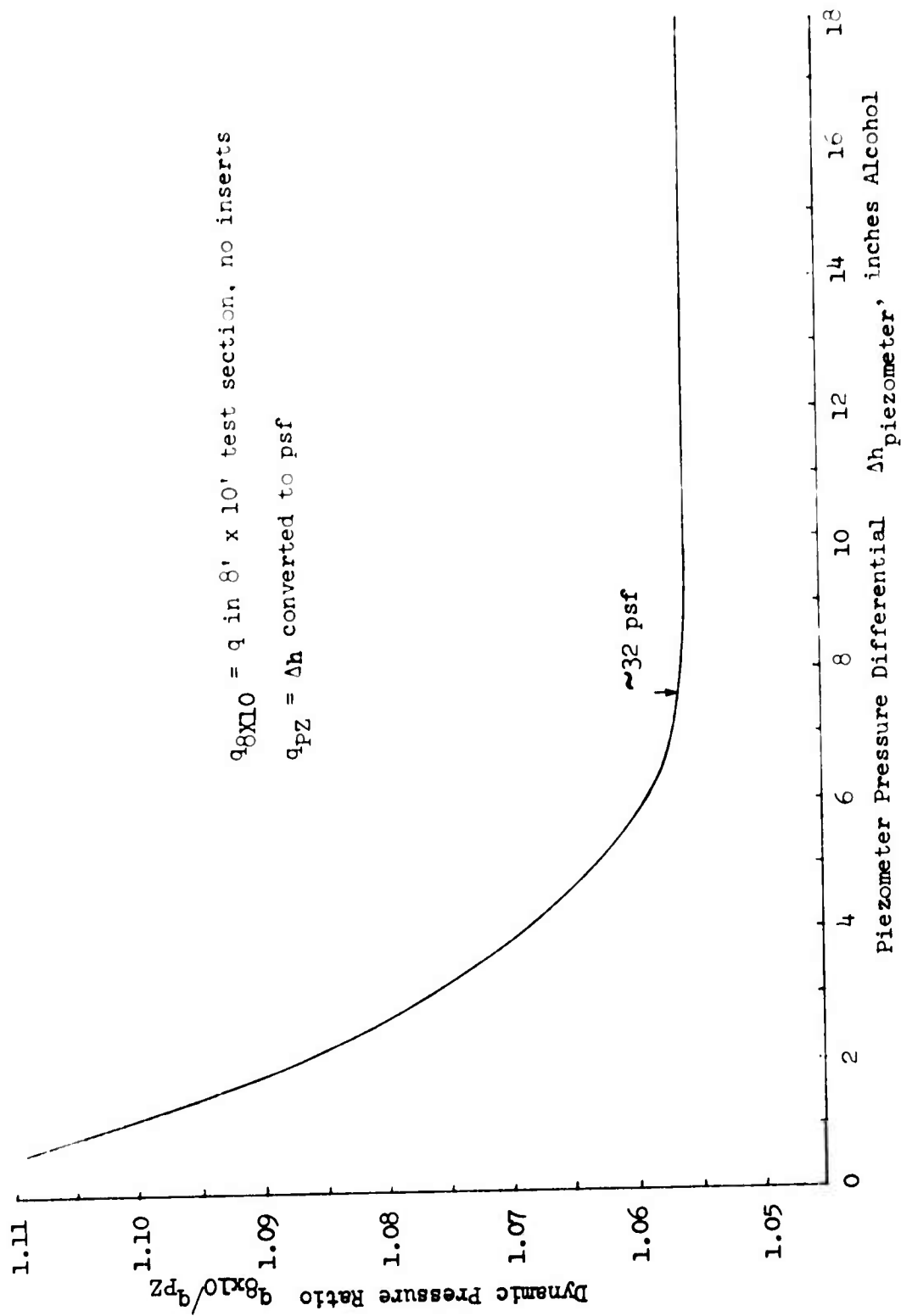
Figure 4 - Correlation Between Piezometer Ring and Dynamic Pressure in the 8' x 10' Test Section.
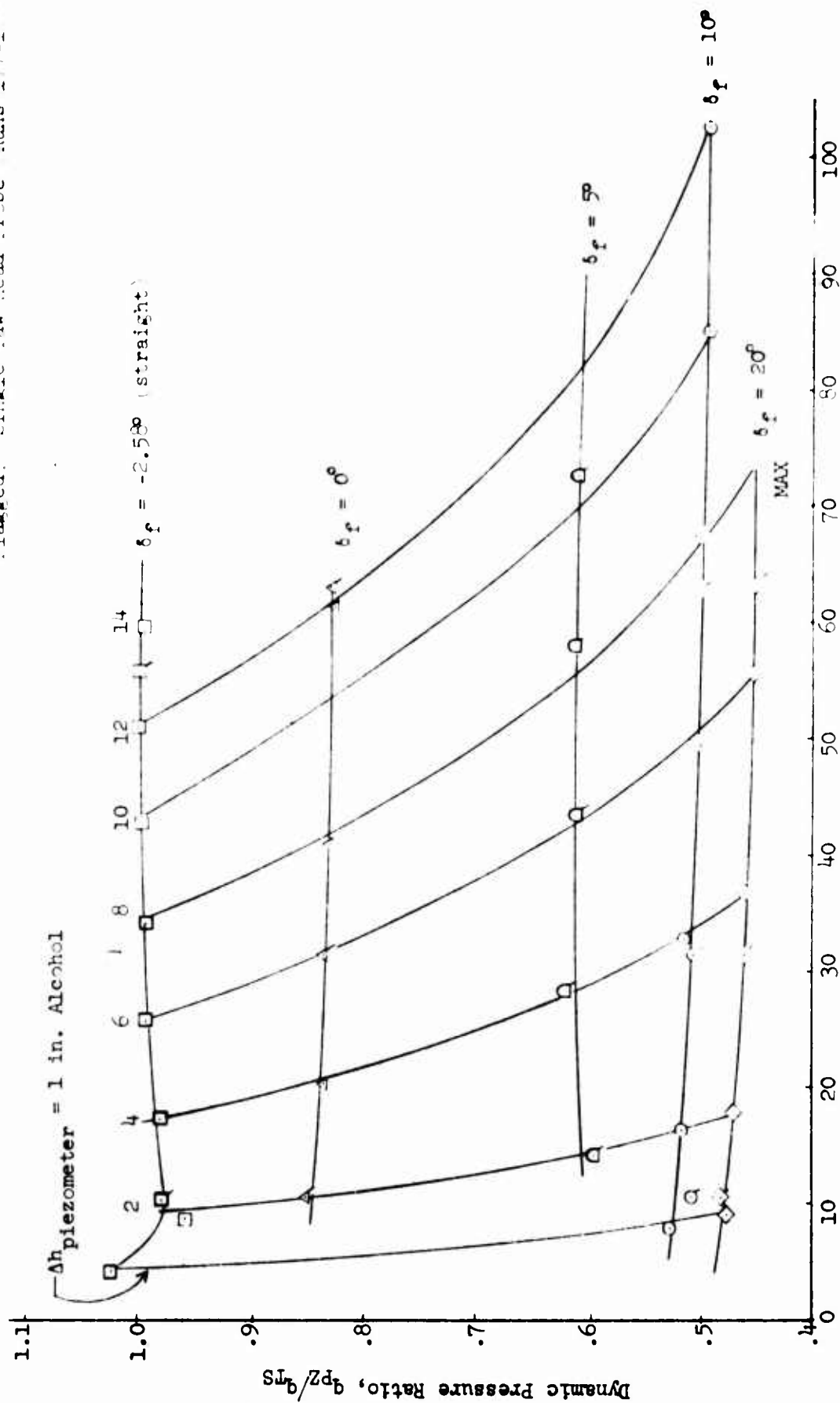
Figure 5 - Empty Test Section Calibration
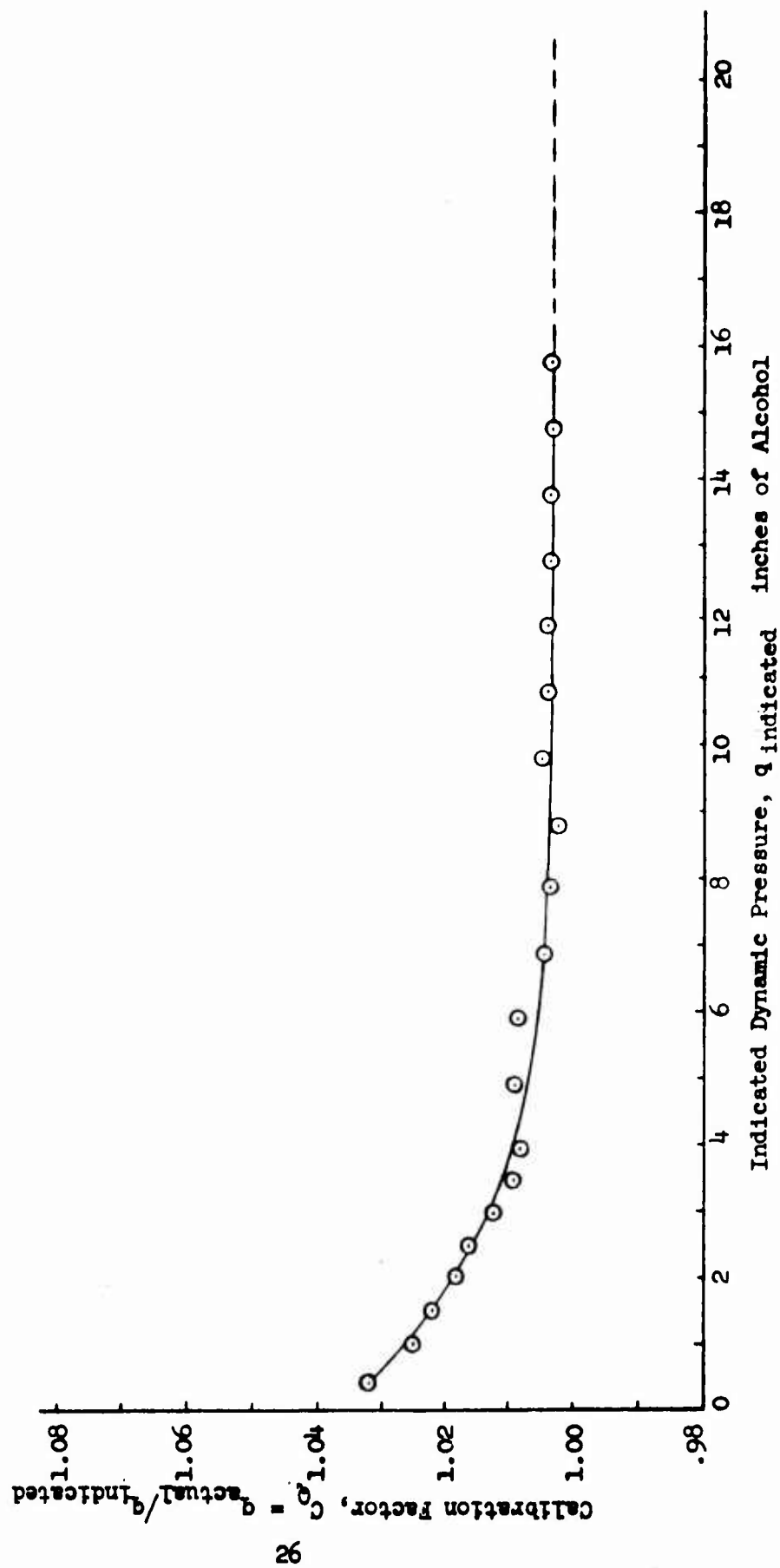
Figure 6 - Pitot-Static Probe Calibration

26
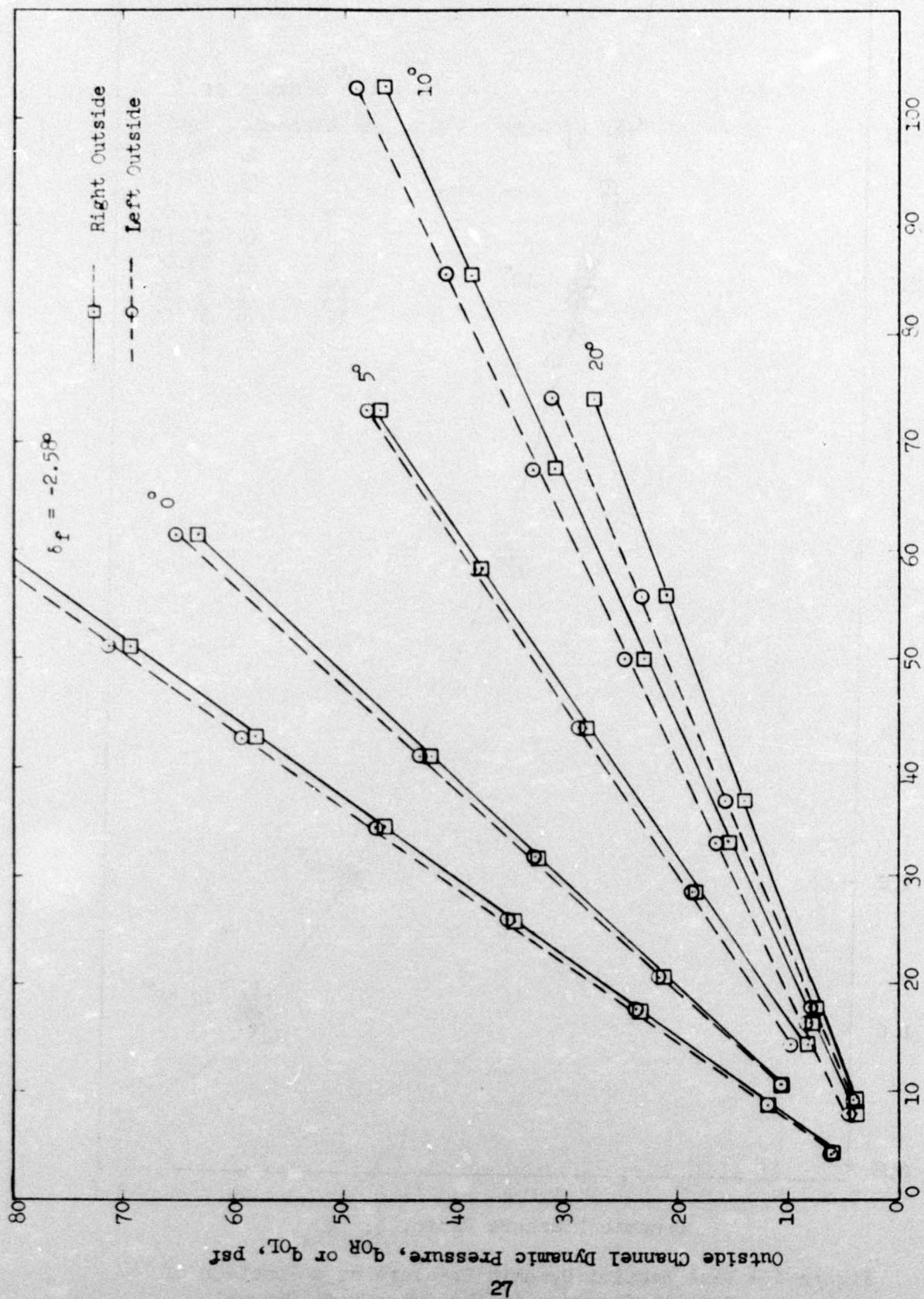
Figure 7 - Dynamic Pressure in the Outside Channels
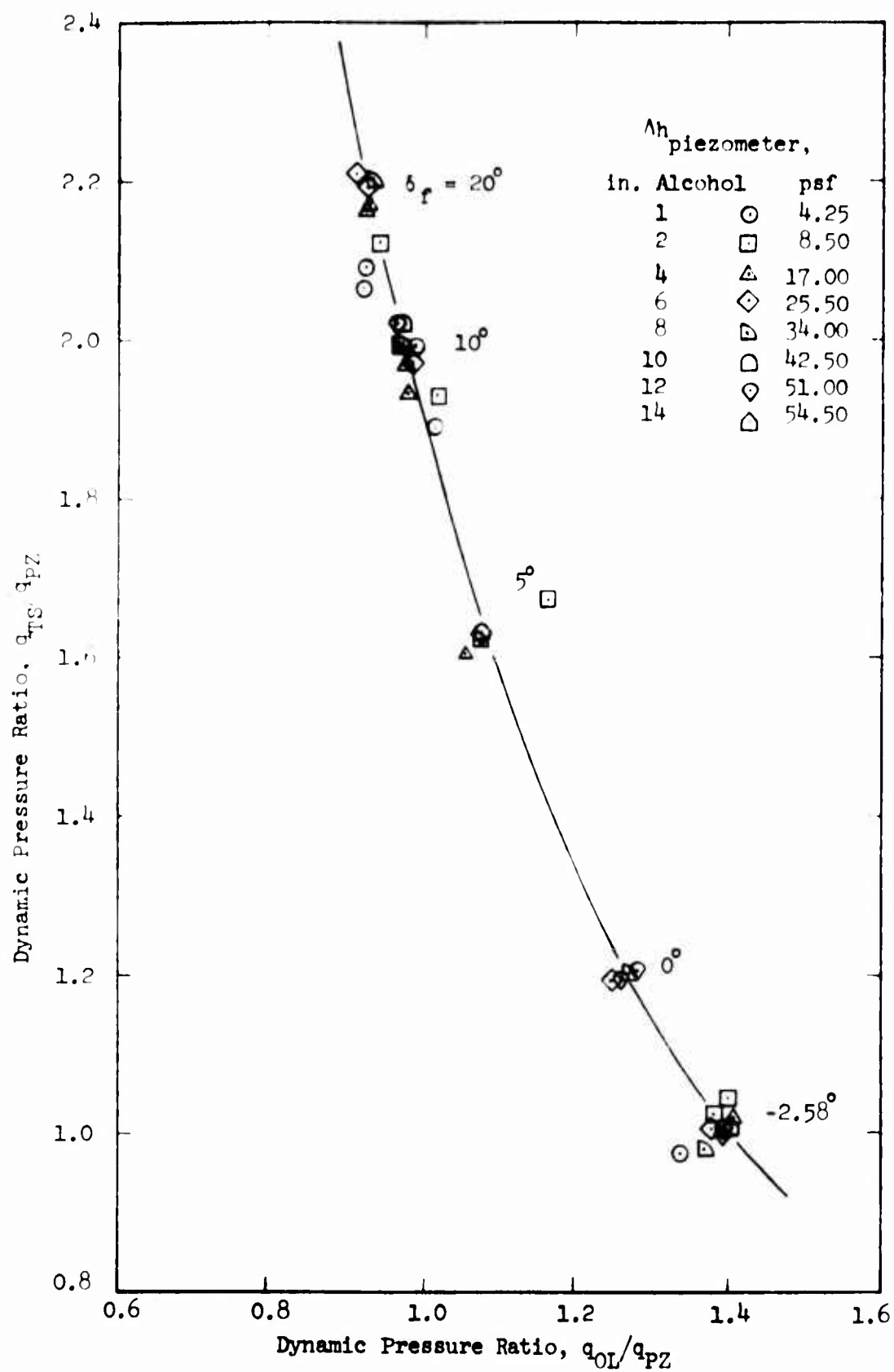
Figure 8 - Test Section Dynamic Pressure as a Function of
Dynamic Pressure in the Outer Left Channel
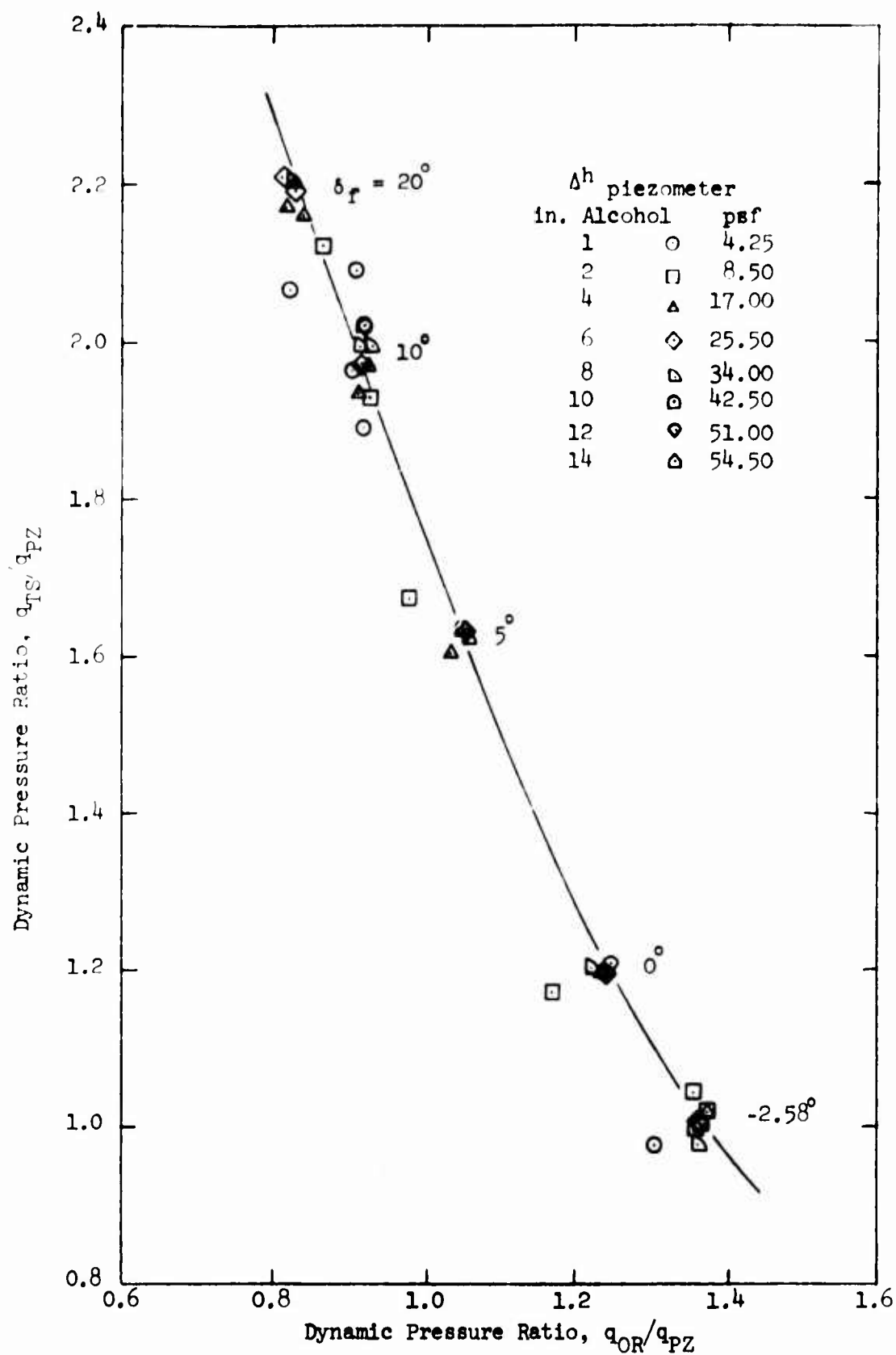
Figure 9 - Test Section Dynamic Pressure as a Function of Dynamic Pressure in the Outer Right Channel
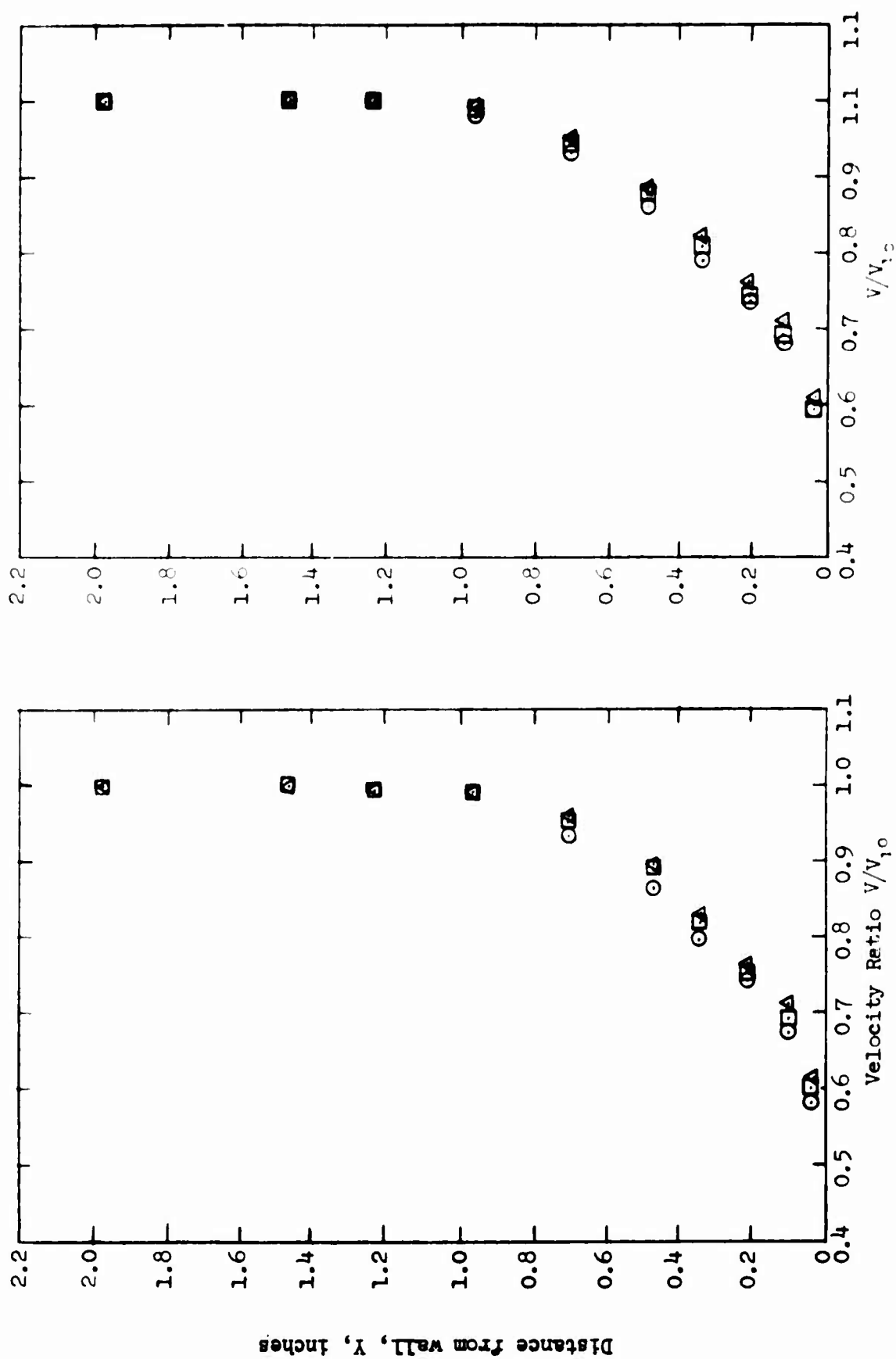
Figure 10 - Boundary Layer Velocity Profiles 12" Upstream of Tunnel Centerline
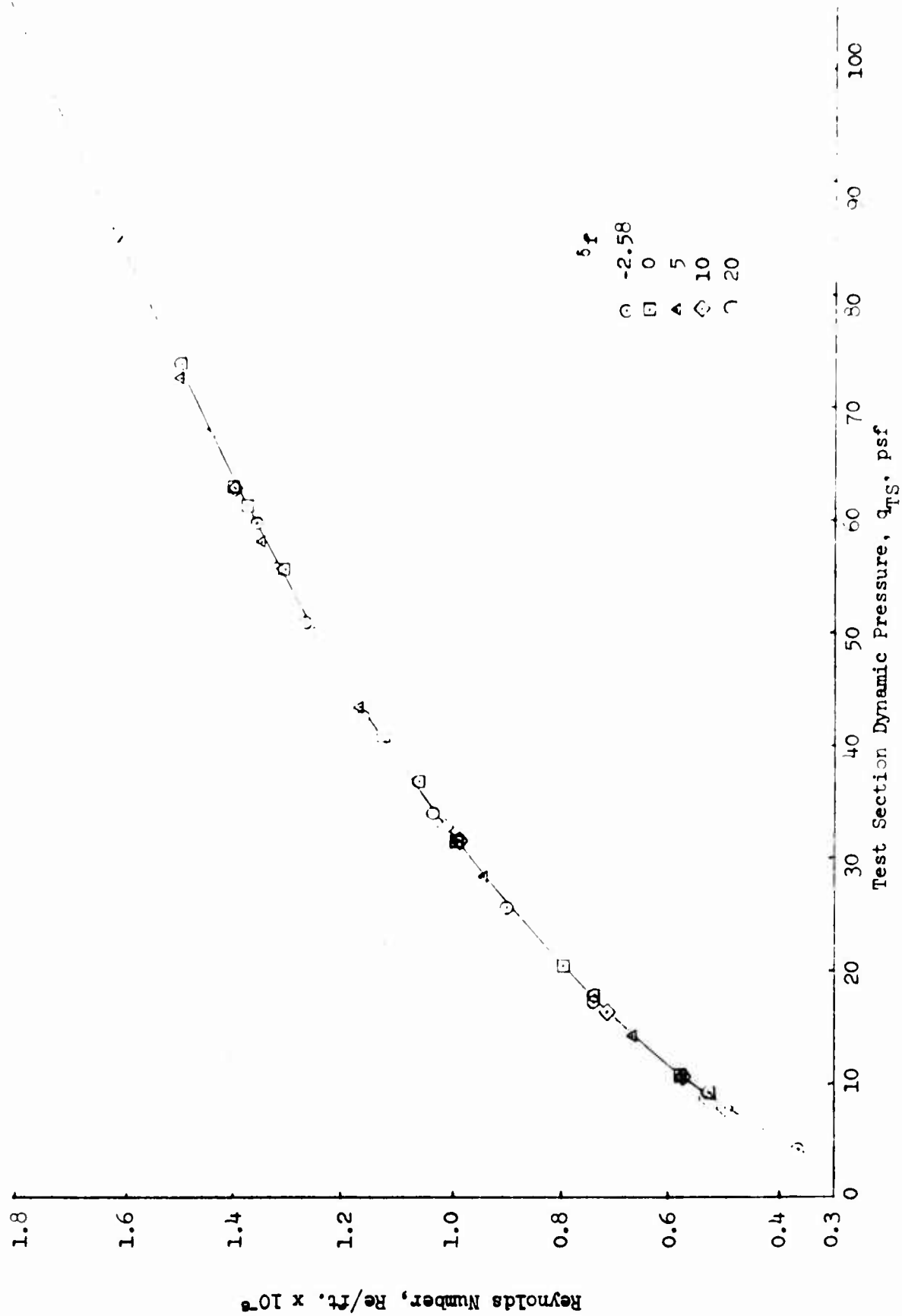
Figure 11 - Test Section Reynolds Number Per Foot
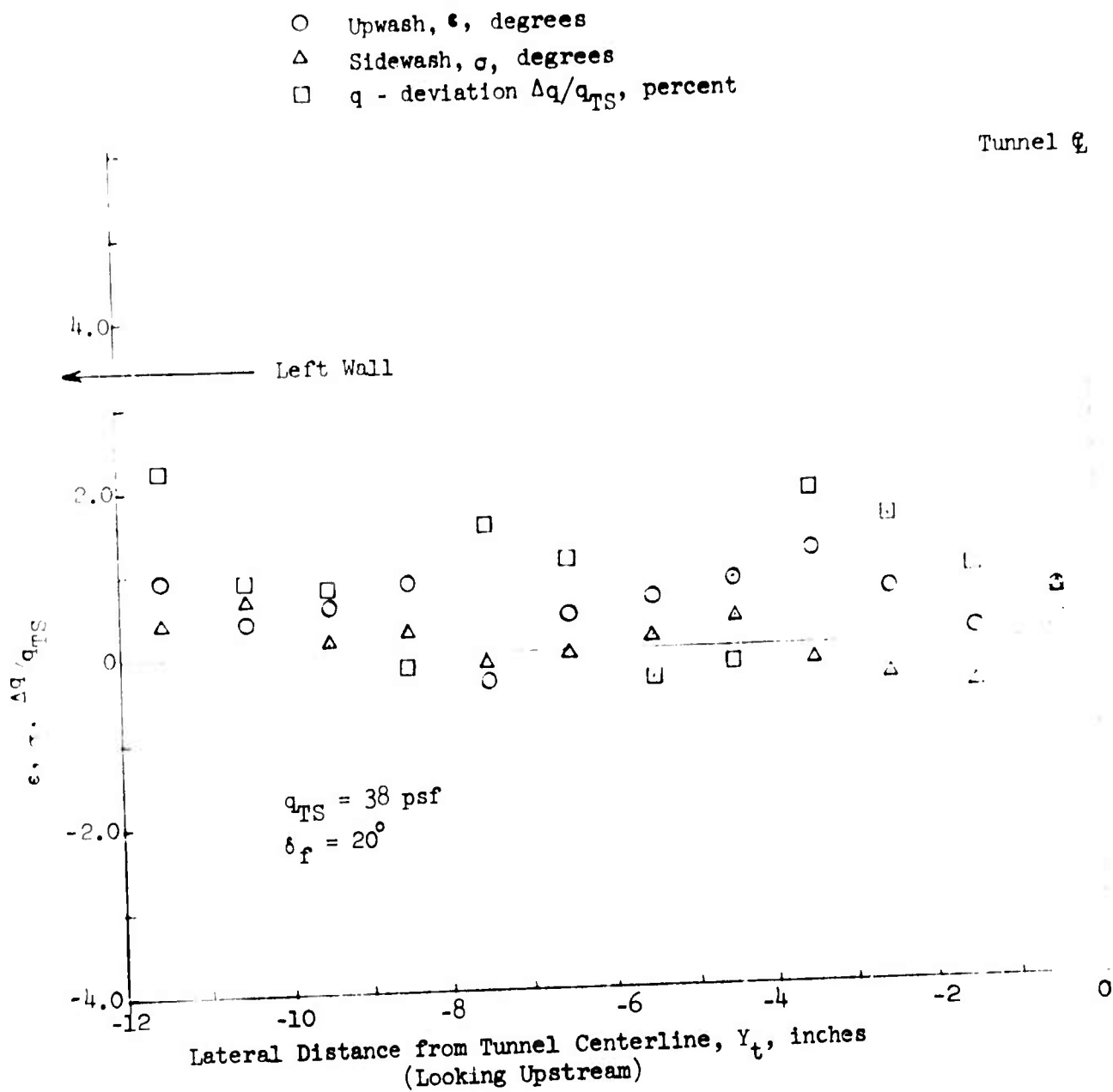
Figure 12 - Sample Angularity and q - Deviation Distributions

32
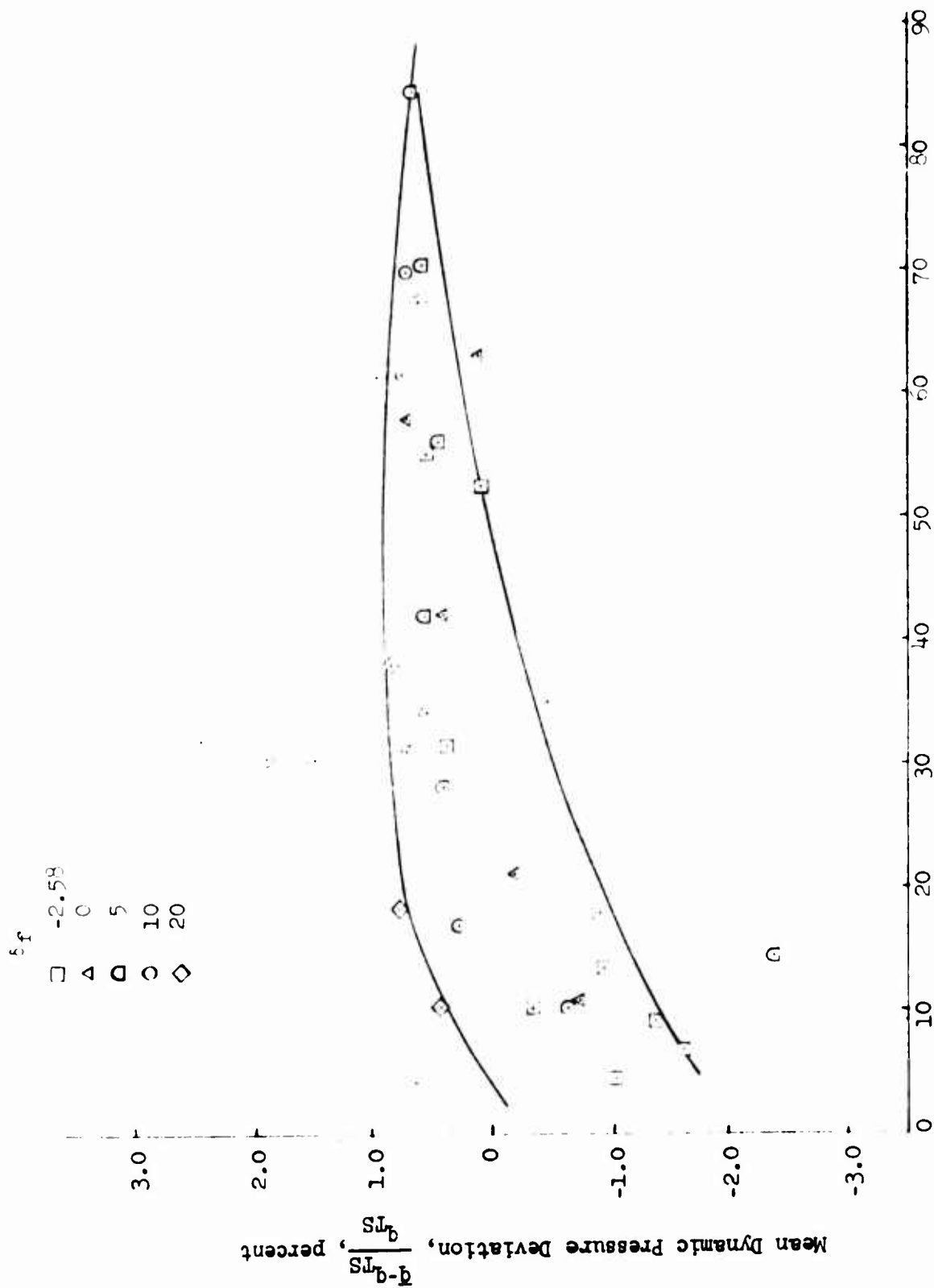
Figure 13 - Mean Spanwise Dynamic Pressure Deviation from the Reference Probe

33
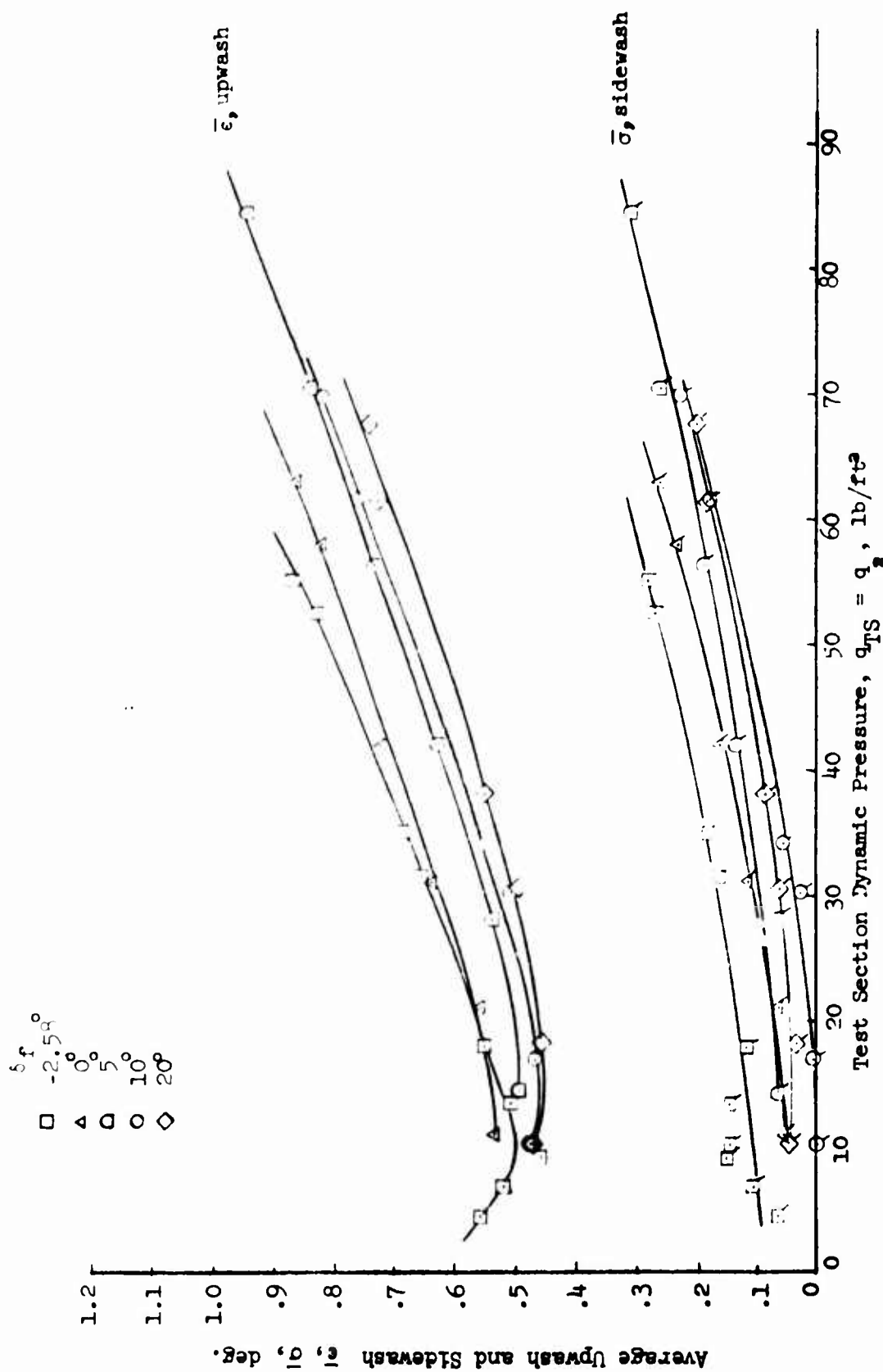
Figure 14 - Indicated Average Variations in Flow Angularity

34
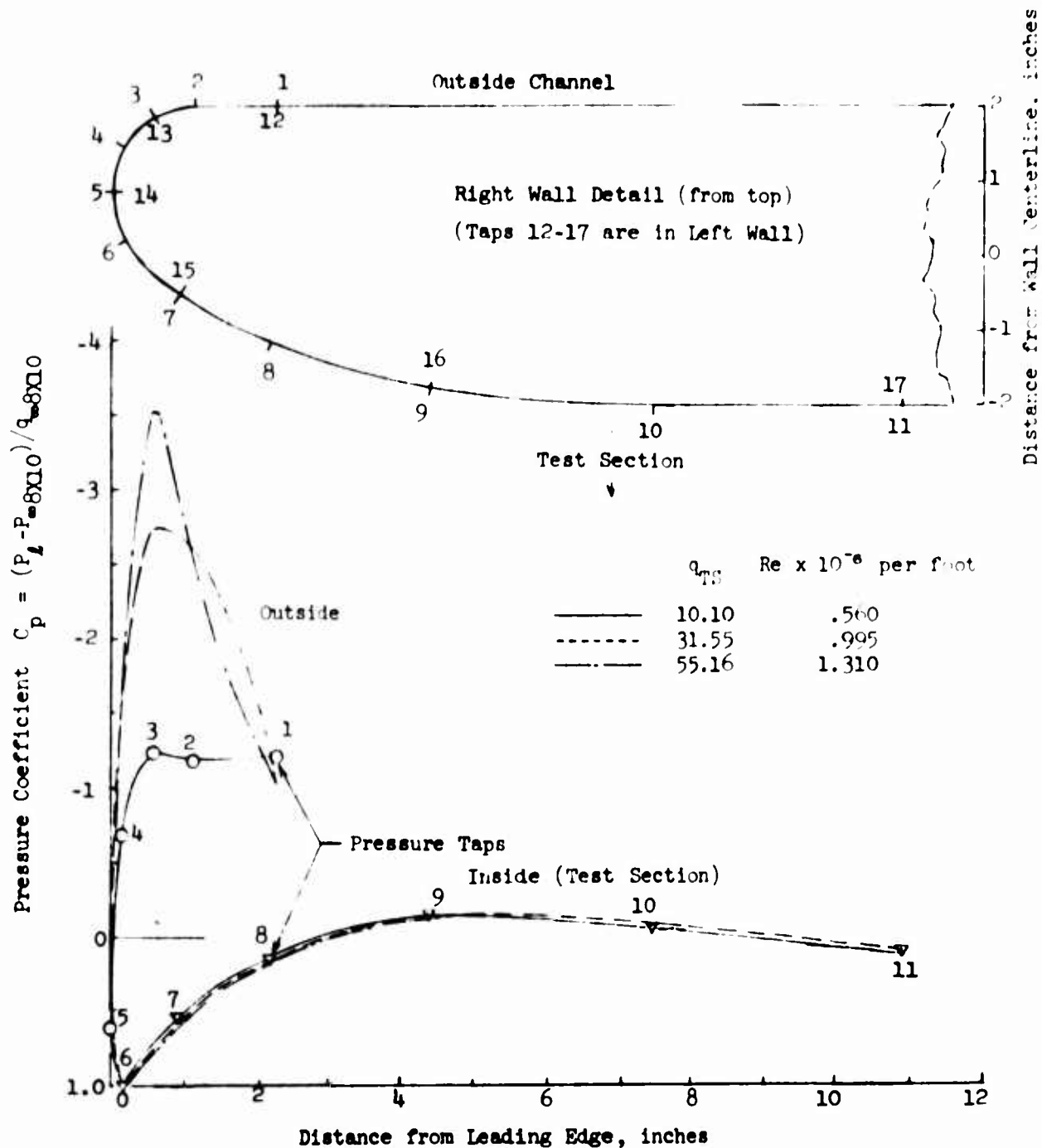
Figure 15 - Leading Edge Pressure Distribution Variation
With Reynolds Number, $\delta_f = -2.58°$

35
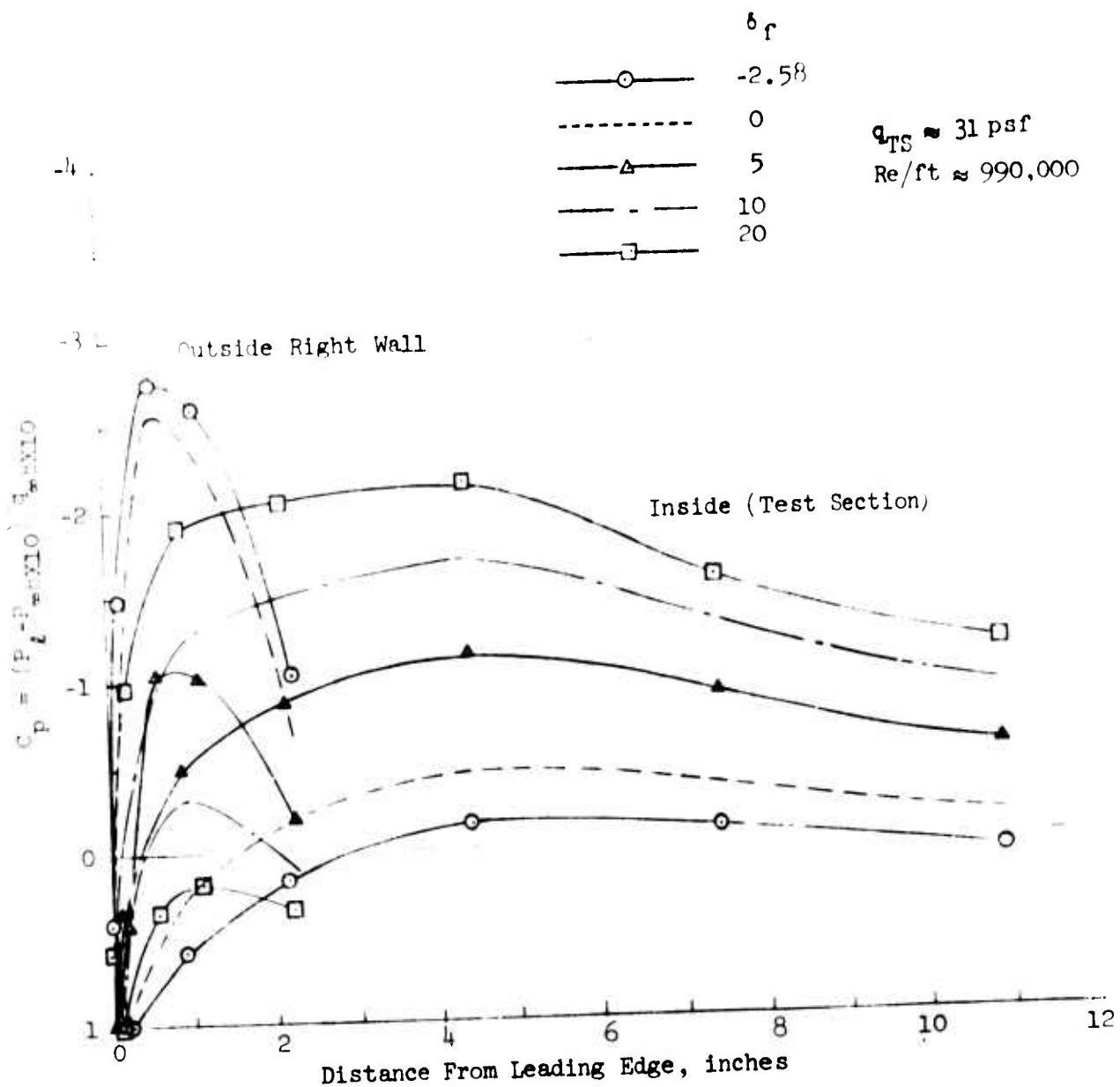
Figure 16 - Effect of Flap Deflection on
Leading Edge Pressure Distribution
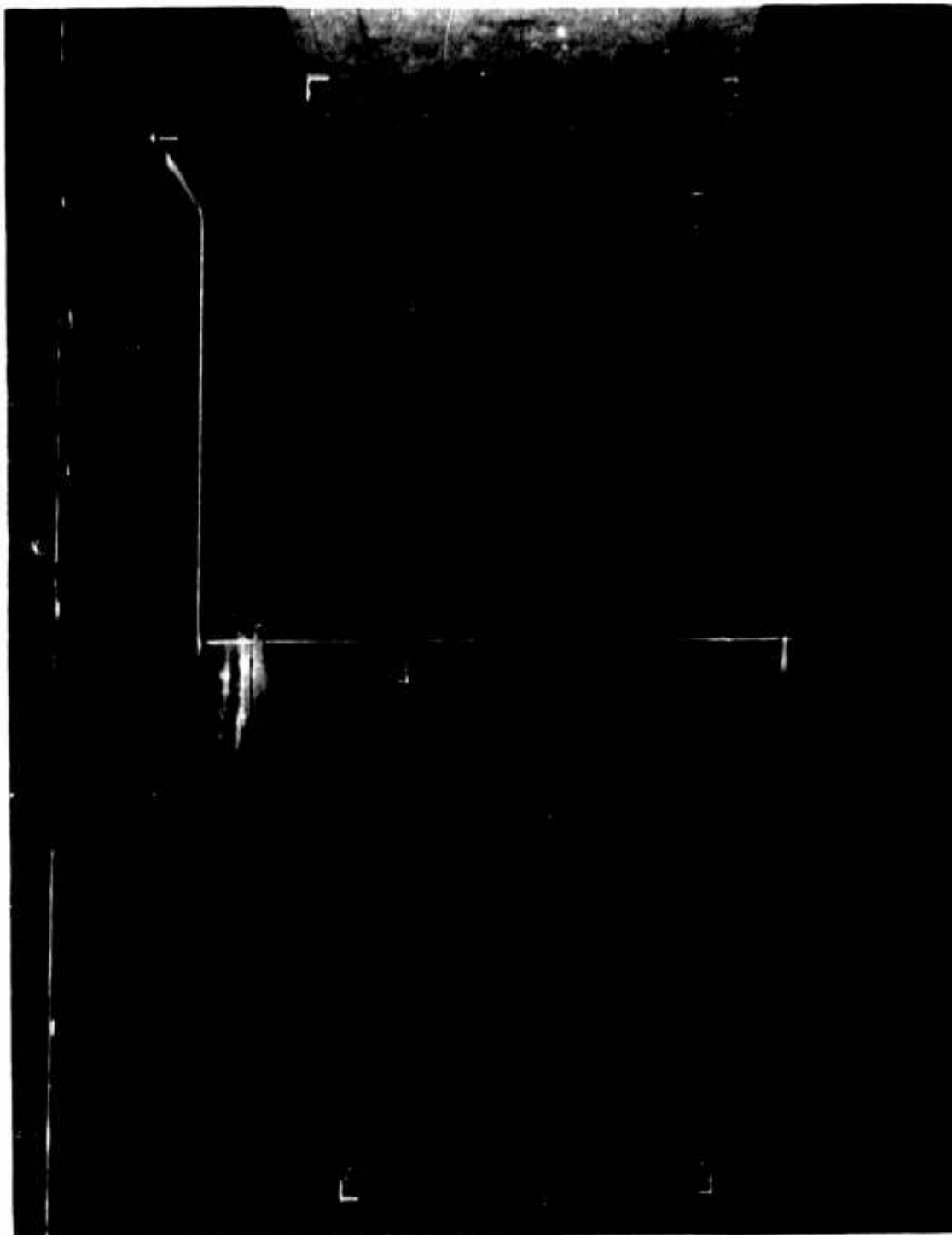
Figure 17 - Two-Dimensional Airfoil and Wake Rake
Installed Between Insert Walls

Figure 18 - Rear View Showing Wake Rake
Detail and Wall Flap Driving Rod
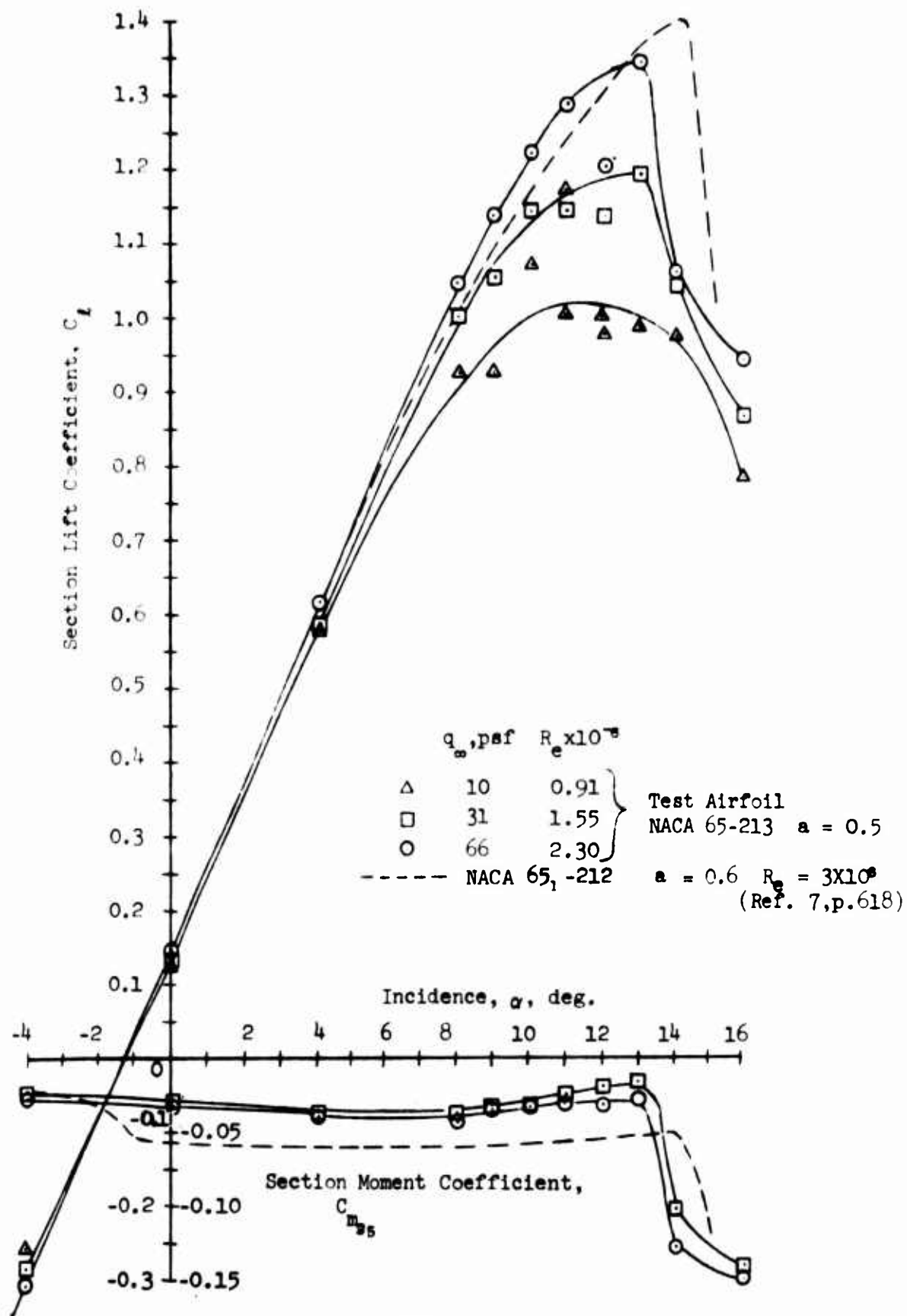
Figure 19 - Lift and Moment Coefficient Variation With
Incidence, NACA 65-213

39
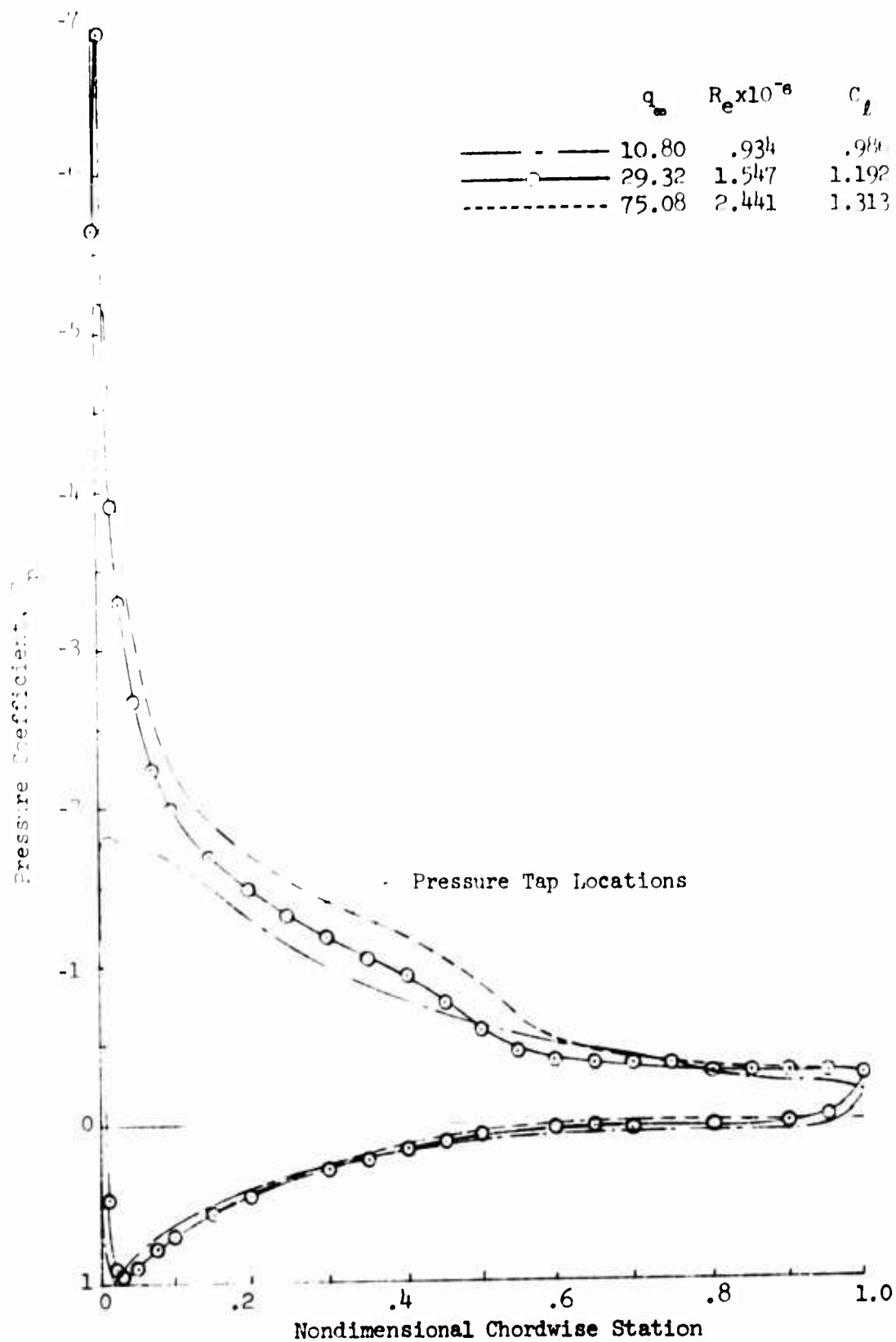
Figure 20 - Reynolds Number Effect on Pressure Distribution,
$\alpha = 13^{\circ}$, NACA 65-213
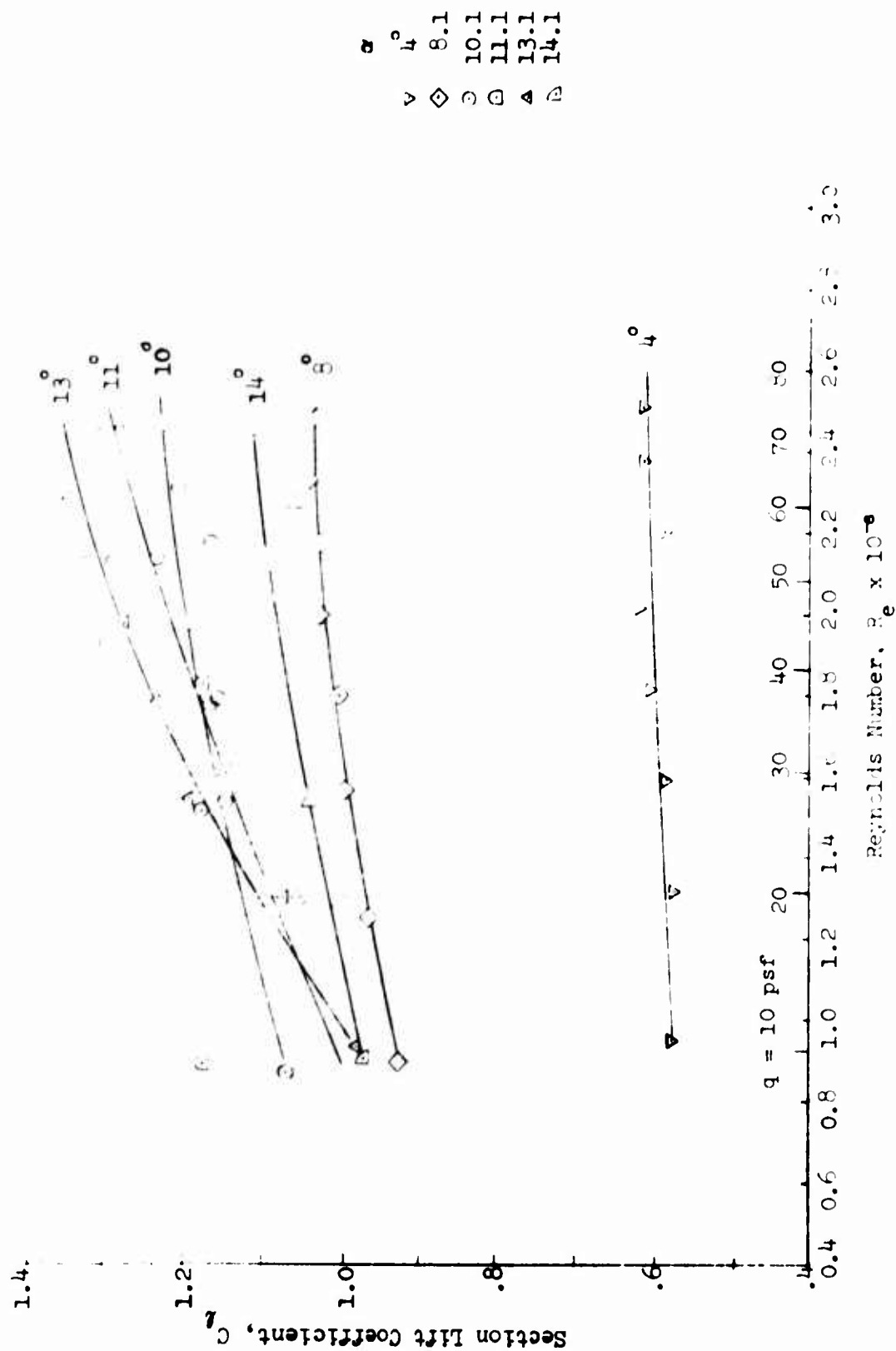
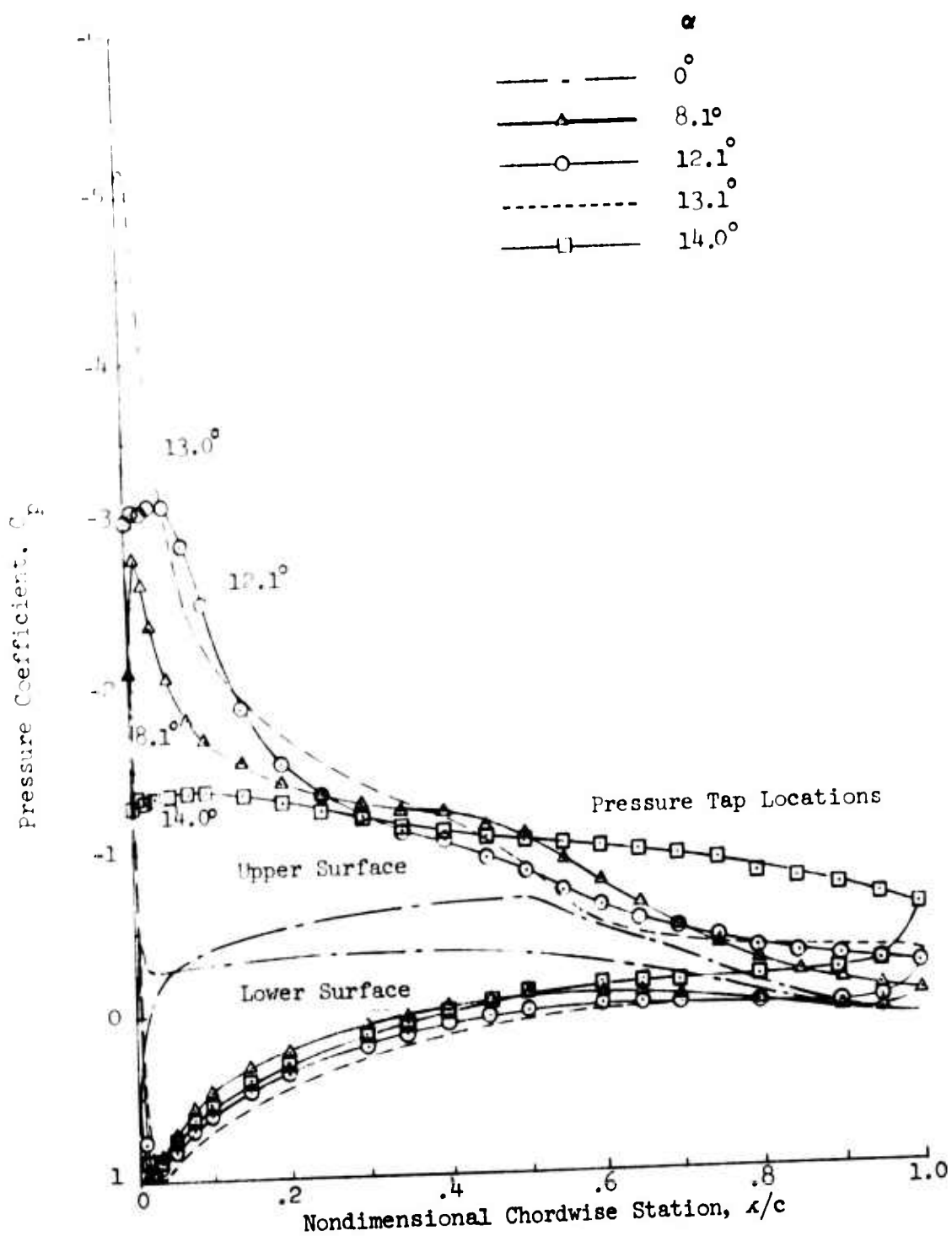Figure 21 - Reynolds Number Effect on Lift Coefficient, NACA 65-213

q = 10 psf

Reynolds Number, R_e x 10^{-6}

Section Lift Coefficient, c_l

α°	
$\triangledown$	4
$\diamondsuit$	8.1
$\bigcirc$	10.1
$\square$	11.1
$\triangle$	13.1
$\square$	14.1

13° 11° 10° 14° 8° 4°

1.4 1.2 1.0 .8 .6

0.4 0.6 0.8 1.0 1.2 1.4 1.6 1.8 2.0 2.2 2.4 2.6 2.8 3.0

20 30 40 50 60 70 80

43

Pressure Coefficient, C_p

α

— · — — 0°

—△— 8.1°

—○— 12.1°

---------- 13.1°

—▢— 14.0°

13.0°

12.1°

8.1°

14.0°

Pressure Tap Locations

Upper Surface

Lower Surface

Nondimensional Chordwise Station, x/c

Figure 22 - Variation of Pressure Distribution With Incidence
$q_\infty = 66$ lb/ft^3, NACA 65-213

42
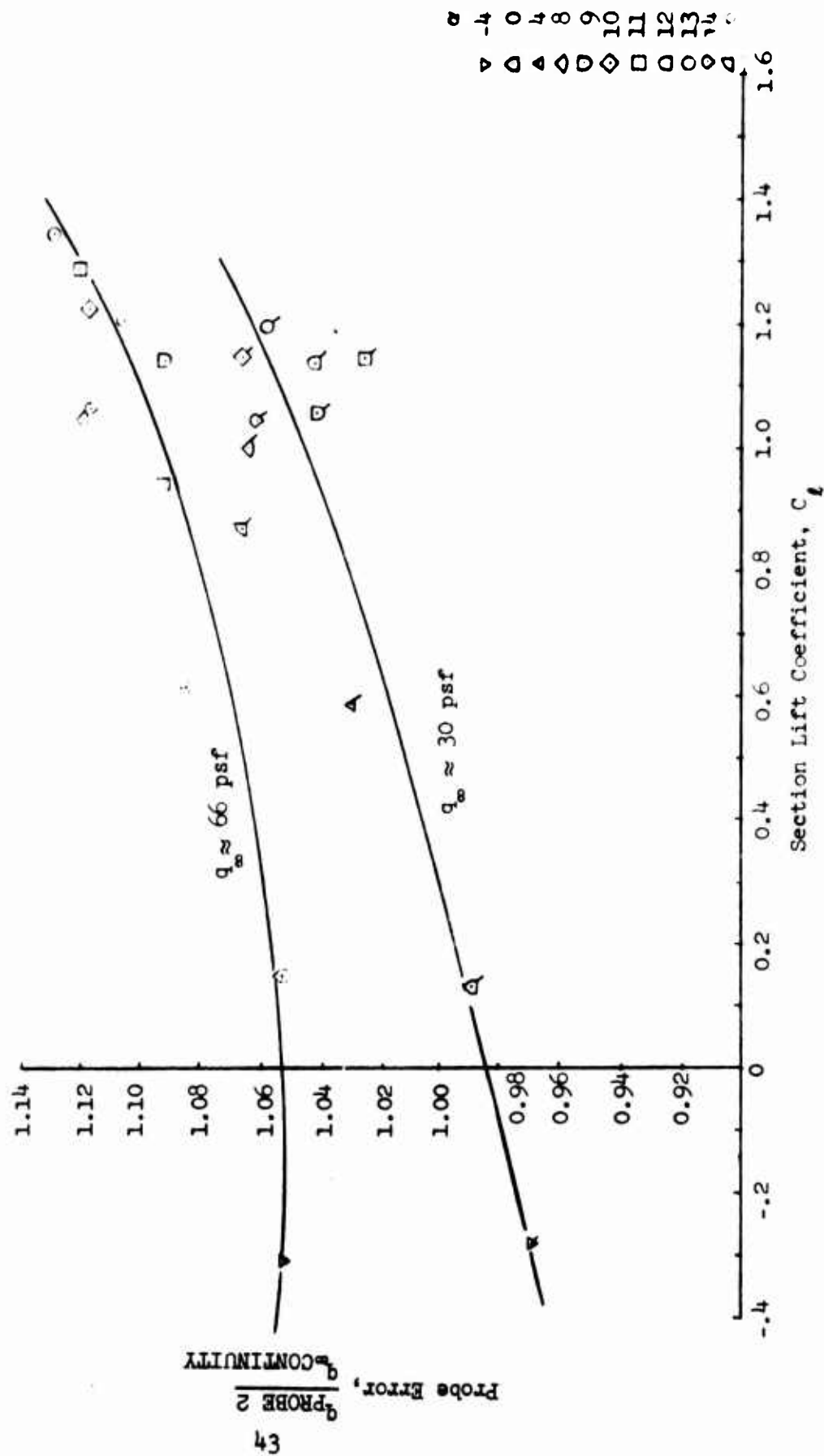
Figure 23 - Test Section Pitot-Static Probe Error as a Function of Lift and Dynamic Pressure, NACA 65-213

43

q_m, psf	$R_e \times 10^{-6}$	
□ 31	1.55	NACA 65-213, a = 0.5, Test Airfoil
⊙ 66	2.30	
--------	3.00	Smooth — NACA 65_1-212
— · —	6.00	Standard Roughness — a = 0.5 (Ref. 7, p. 619)

0.024

0.020

0.016

0.012

0.008

0.004

Section Drag Coefficient, C_d

-0.4   0   0.4   0.8   1.2   1.6

Section Lift Coefficient, C_l
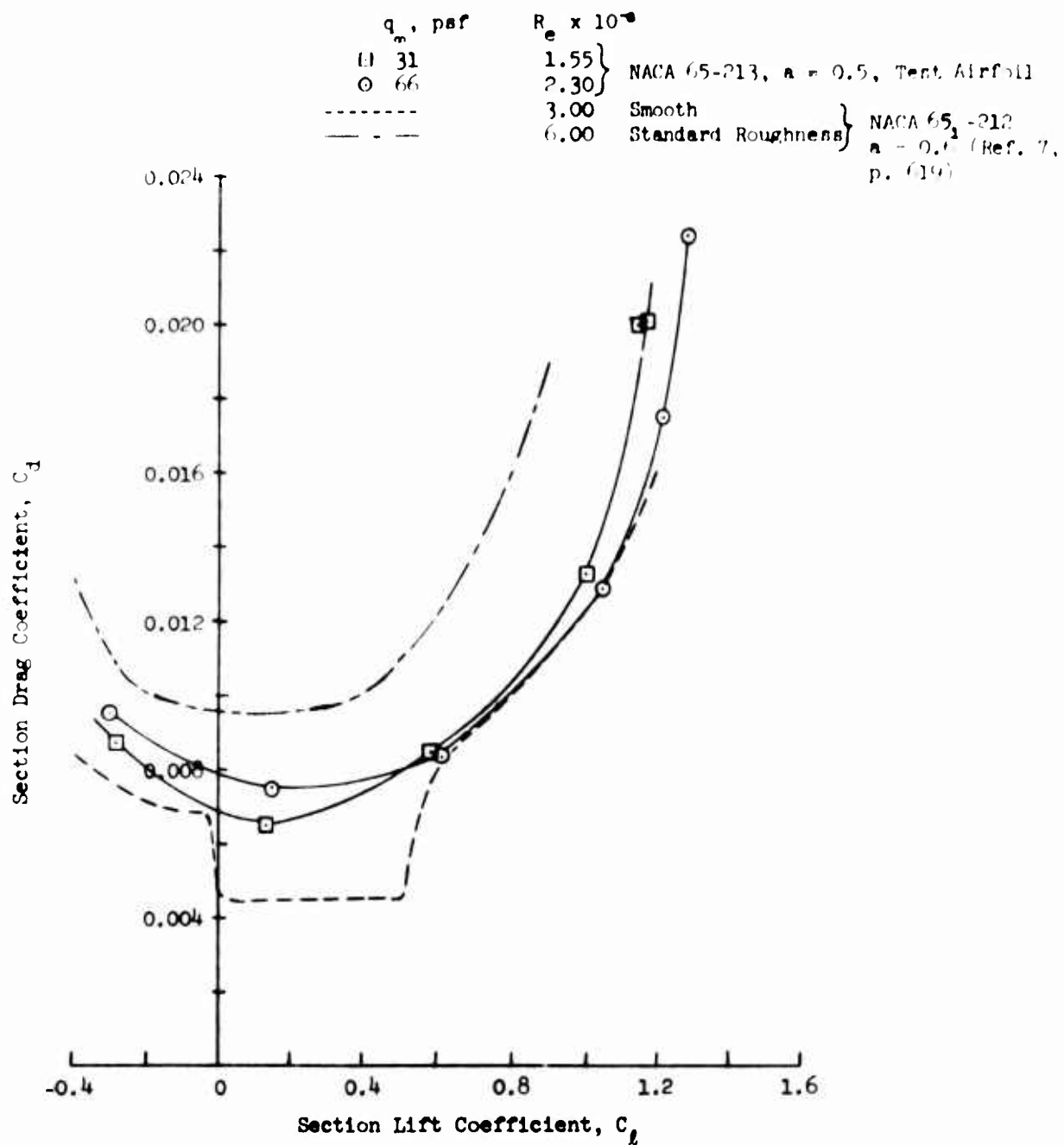
Figure 24 - Drag Polars for the NACA 65-213 at Two Reynolds Numbers

44
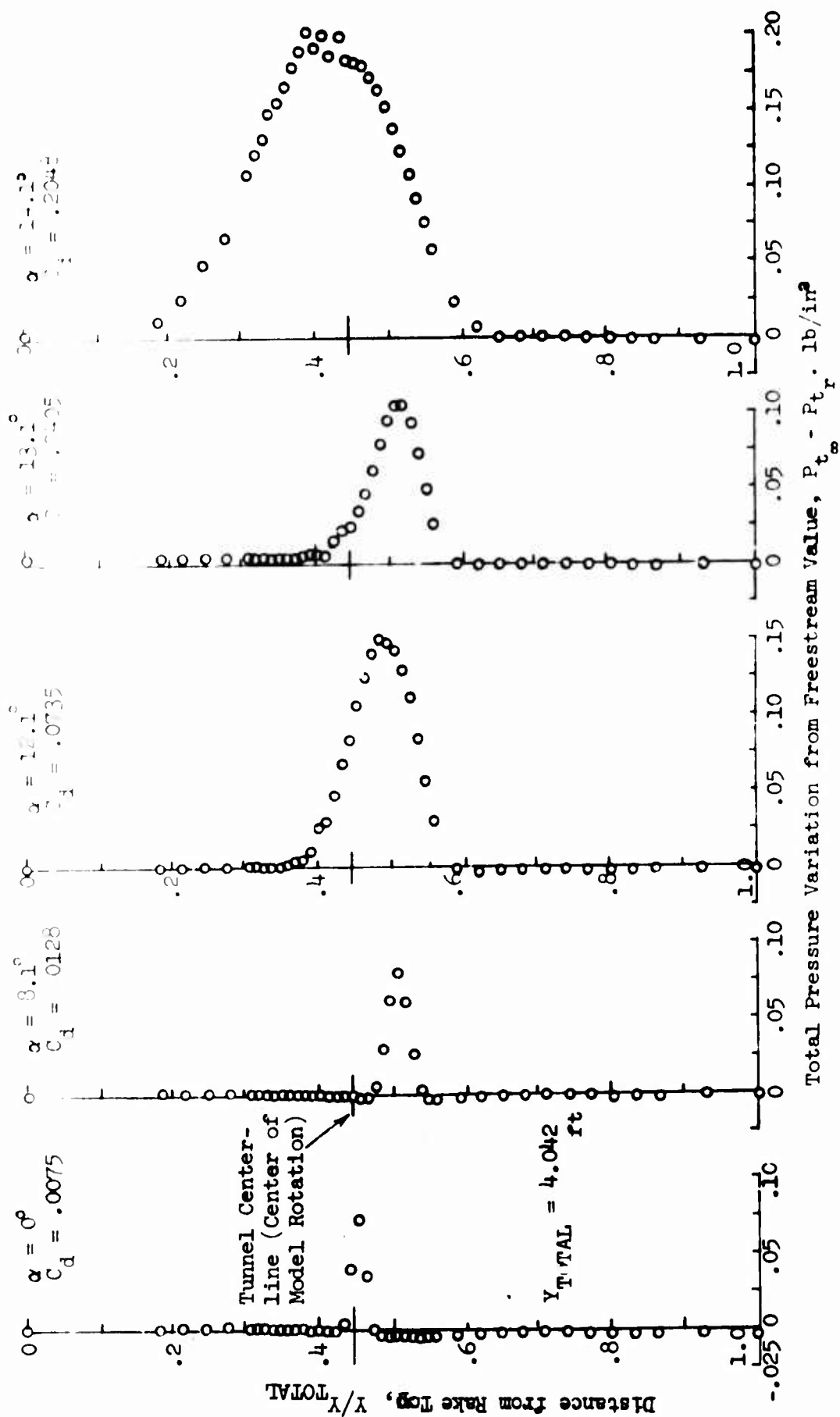
Figure 25 - Variation with Incidence of Wake Rake Total Pressure Distributions, $q_\infty \approx 66$ lb/ft²
NACA 65-213

45
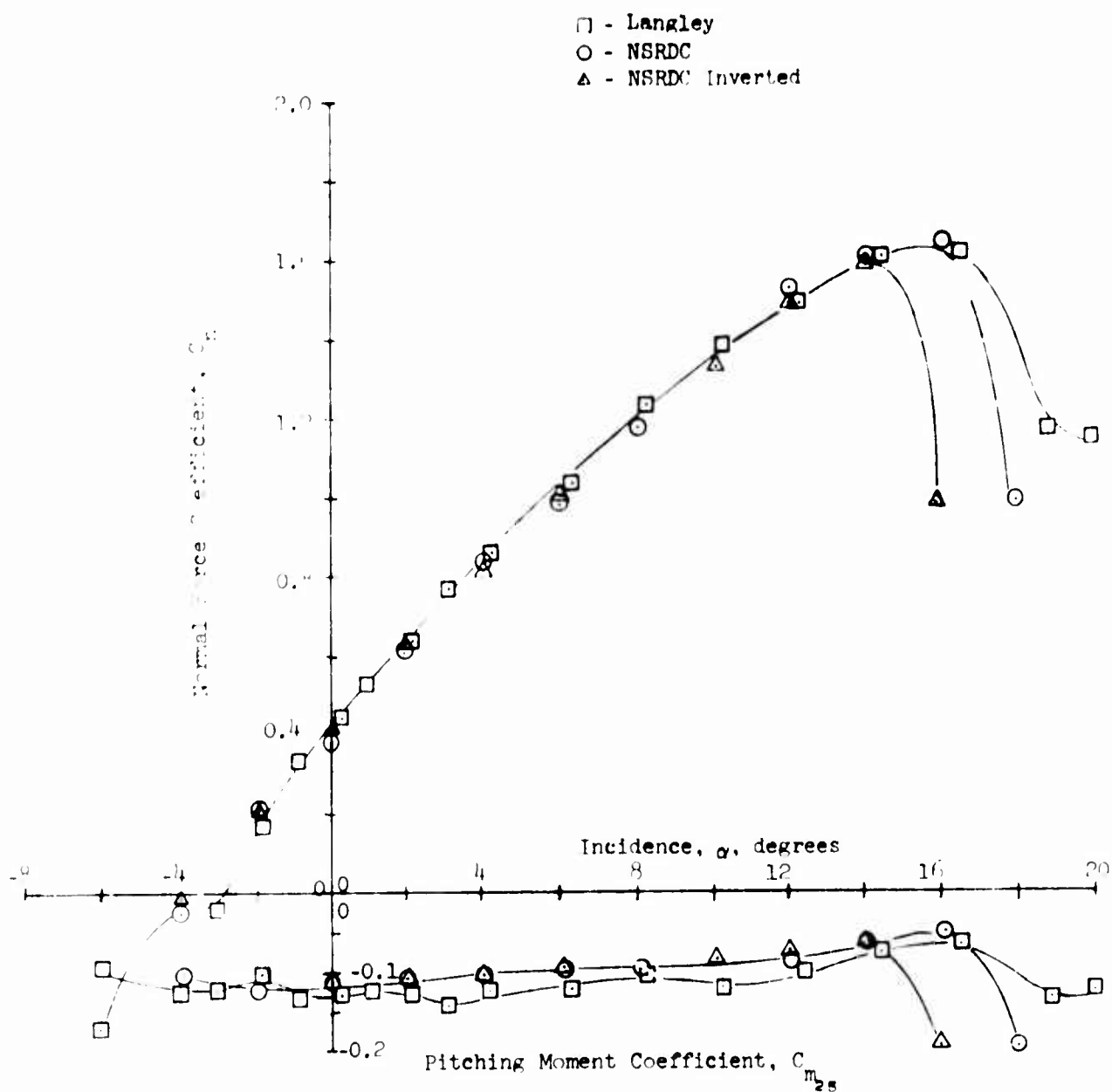
Figure 26 - Normal Force and Moment Coefficient Variation
with Incidence, NASA Reference Section, q_∞ = 32 psf

46
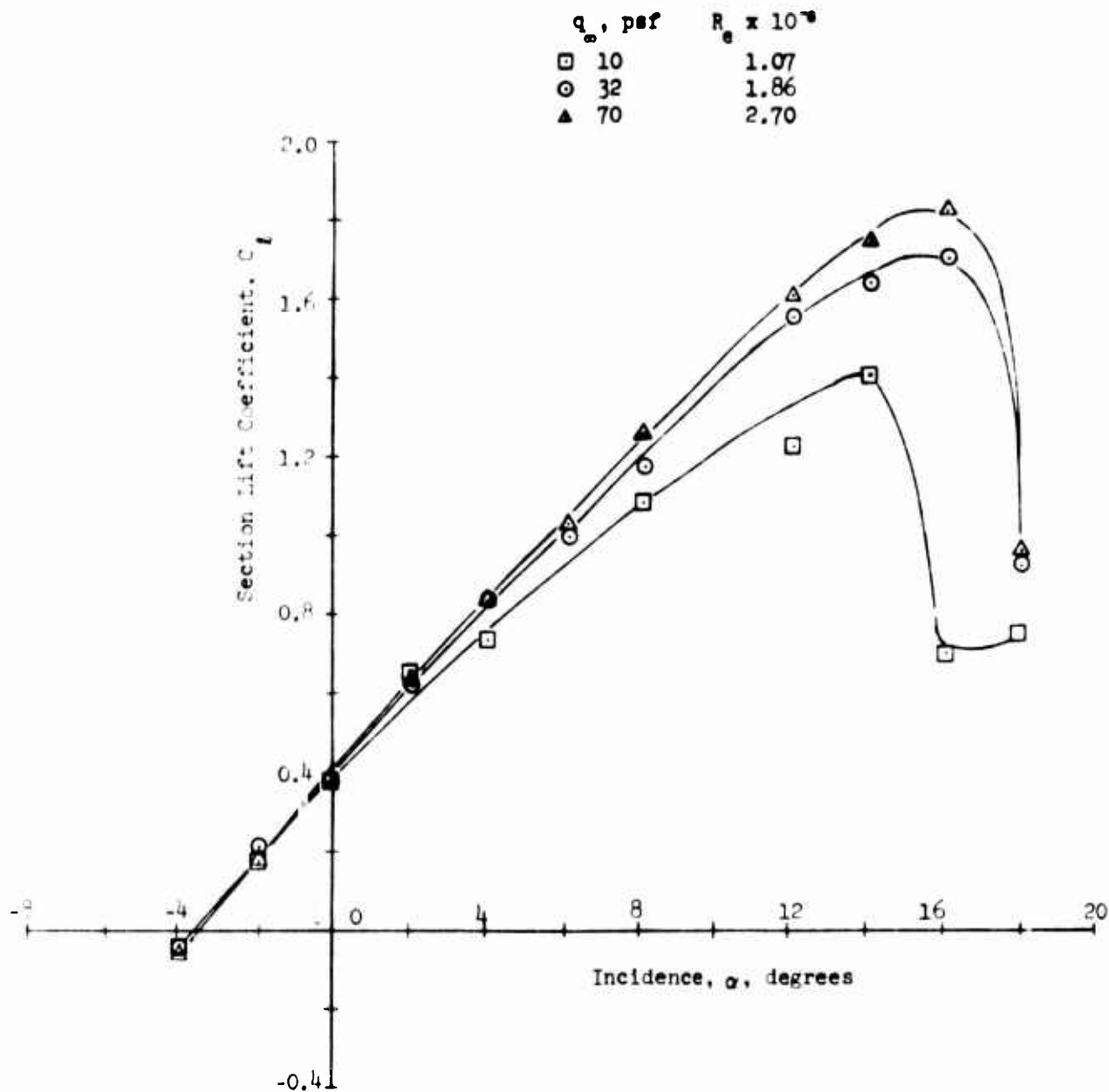
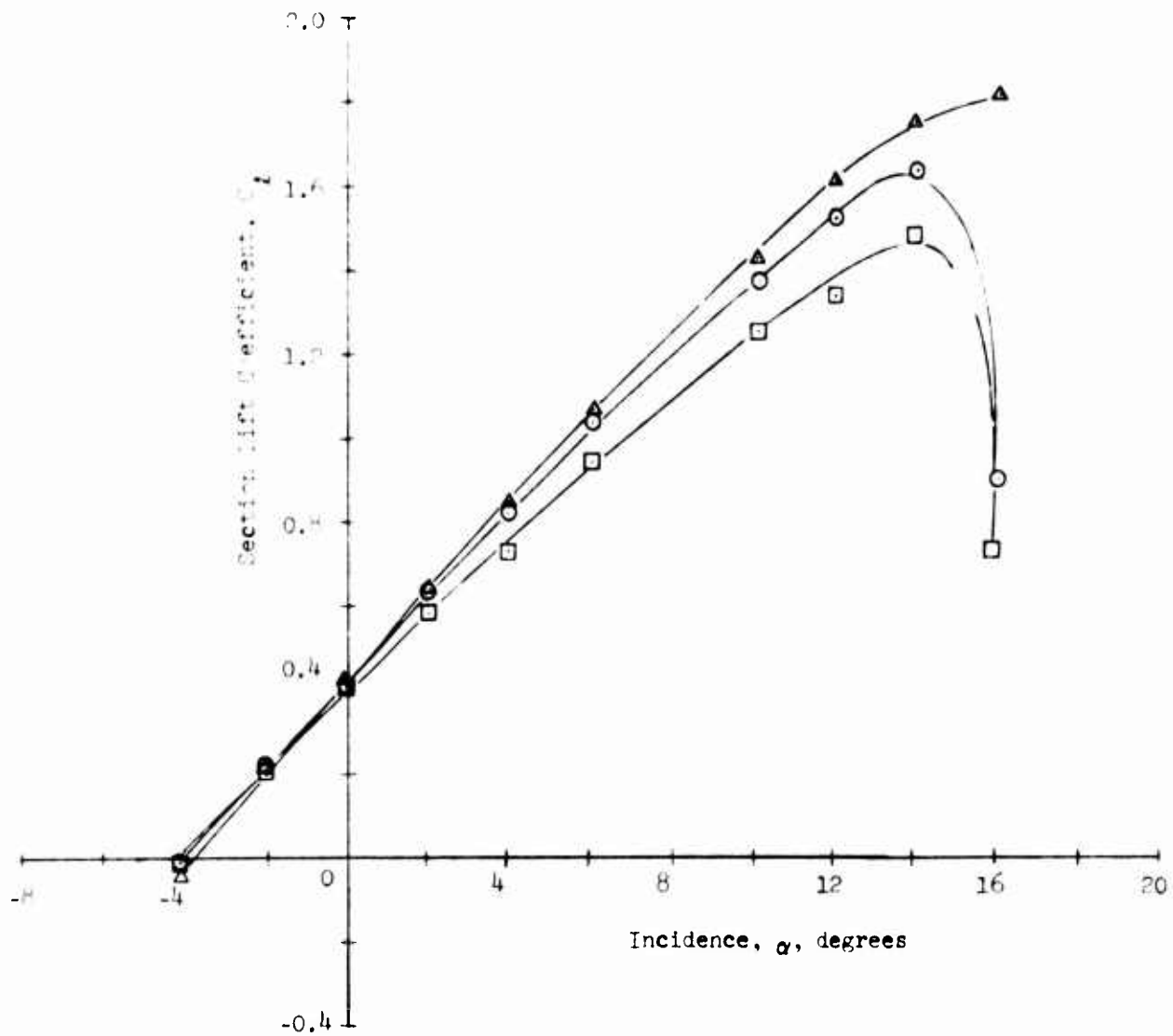Figure 27 - Variation in Lift Curve with Reynolds Number,
Upright NASA Reference Section

Figure 28 - Variation in Lift Curve with Reynolds Number,
Inverted NASA Reference Section
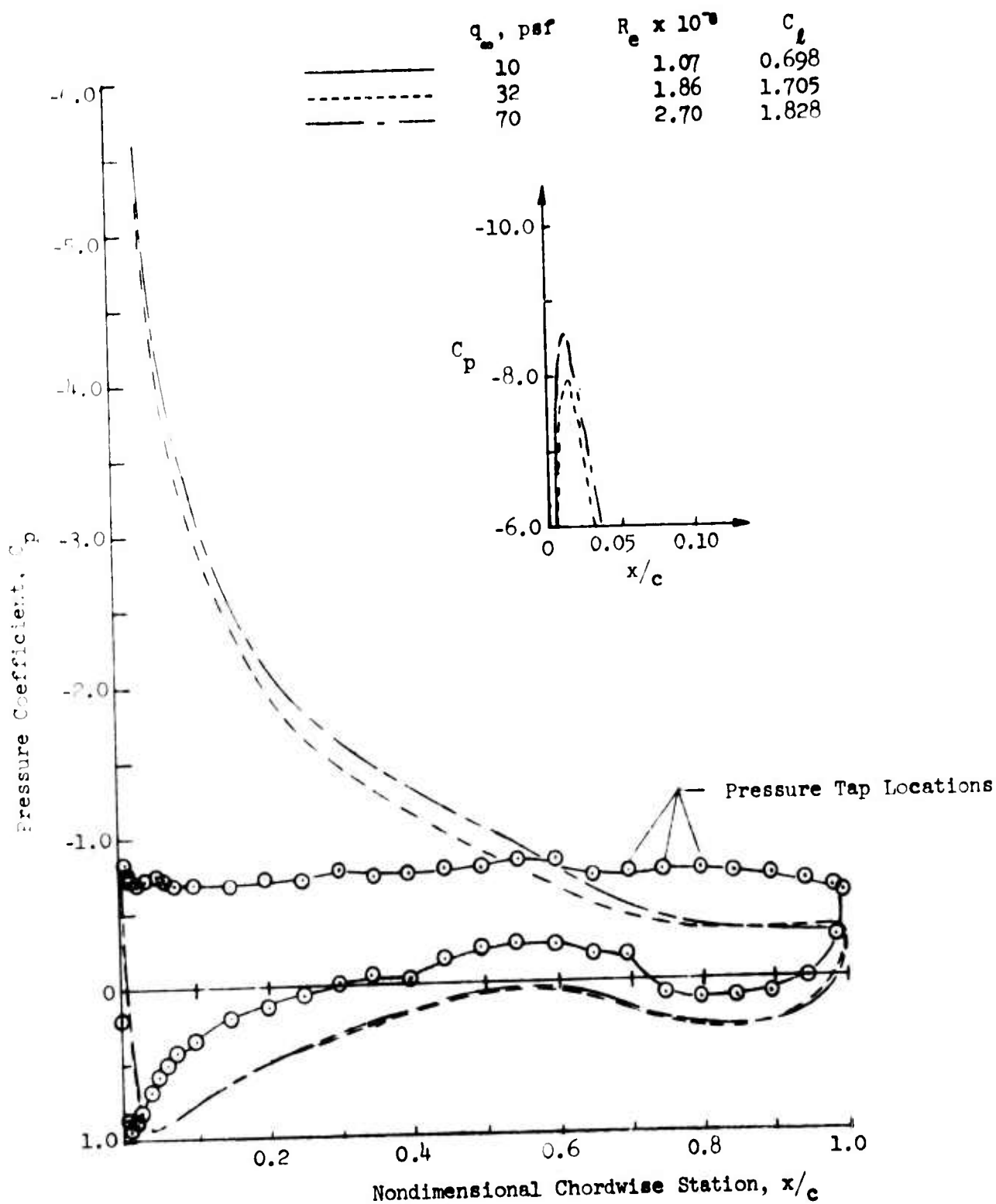
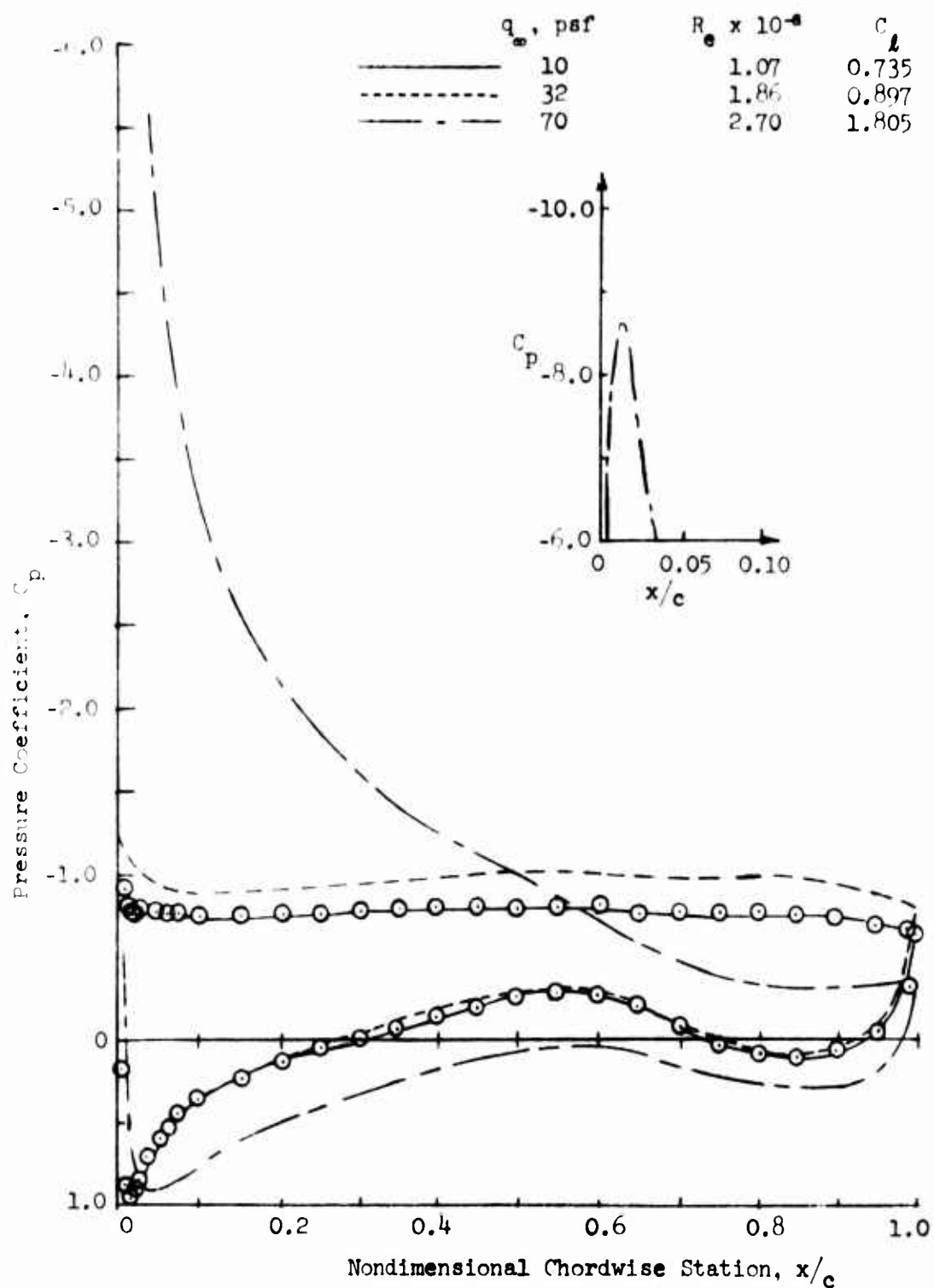Figure 29 - Variation in Pressure Distribution with Reynolds Number, Upright NASA Reference Section at $\alpha = 16$

Figure 30 - Variation in Pressure Distribution with Reynolds Number,
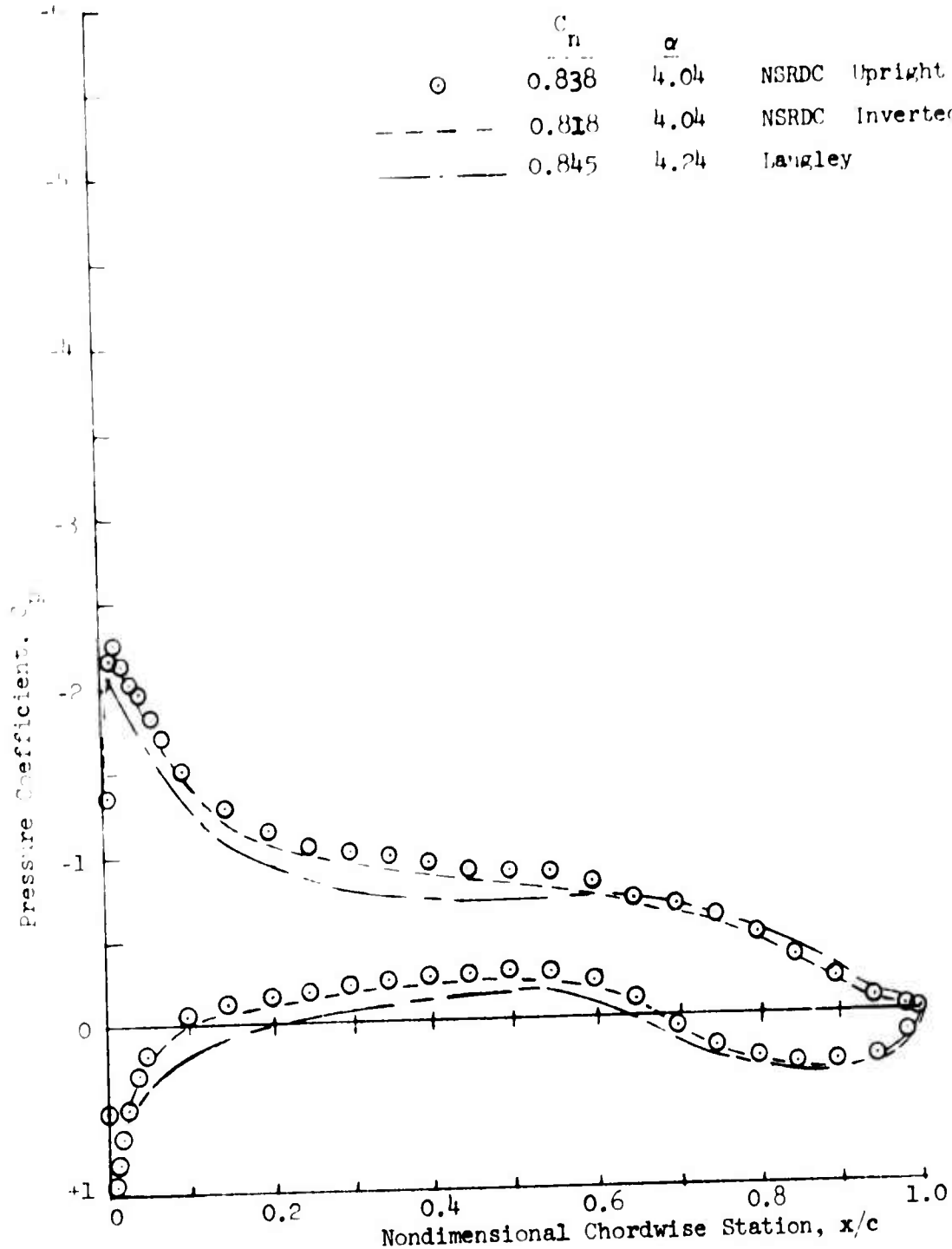Inverted NASA Reference Section, $\alpha = 16^\circ$

Figure 31 - Comparative Pressure Distributions, $\alpha \approx 4°$, $q_\infty \approx 32$ lb/ft^2

51

$$
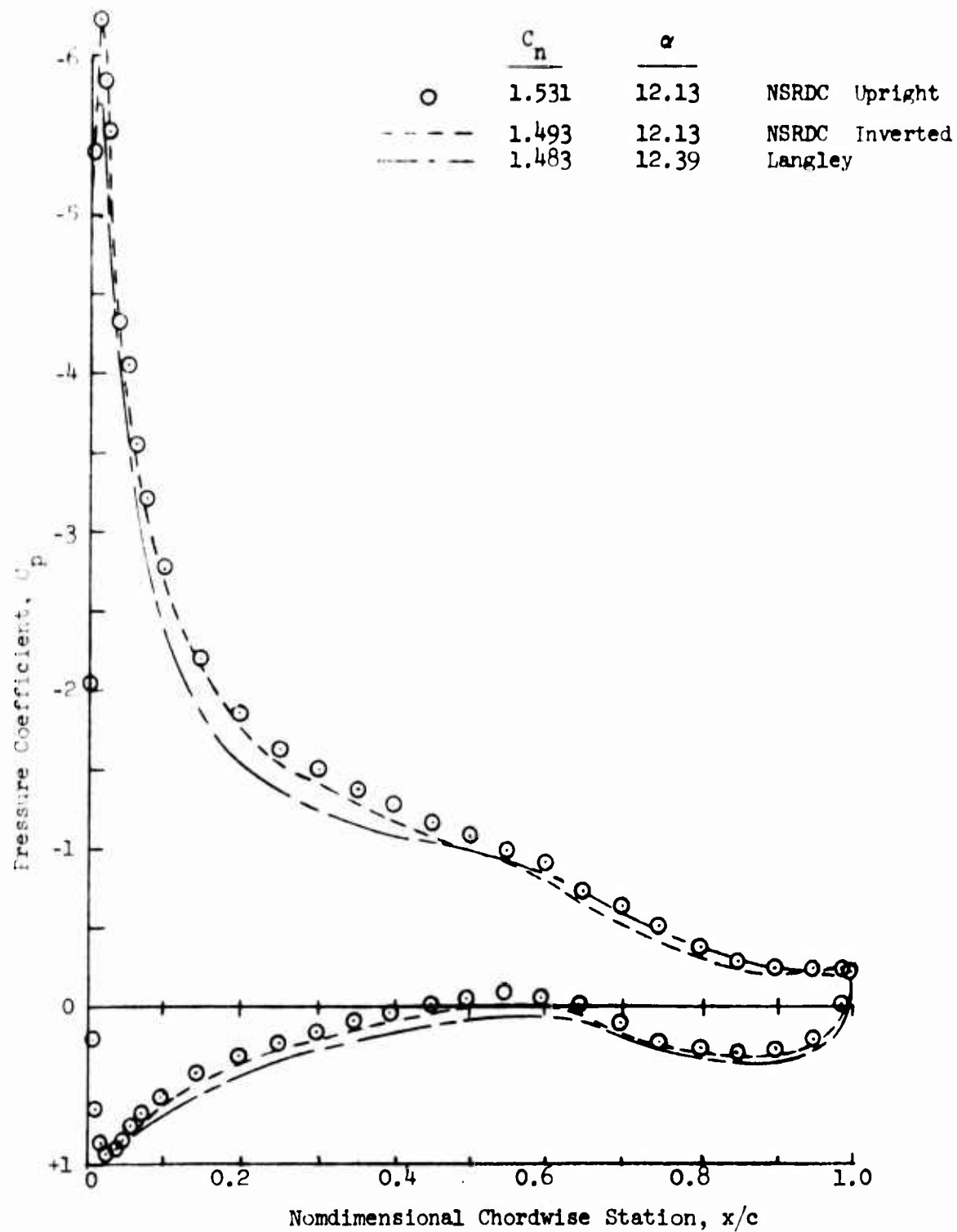\begin{array}{cccl}
 & C_n & \alpha & \\
\hline
\circ & 1.531 & 12.13 & \text{NSRDC Upright} \\
- - - & 1.493 & 12.13 & \text{NSRDC Inverted} \\
-\cdot-\cdot- & 1.483 & 12.39 & \text{Langley}
\end{array}
$$

Pressure Coefficient, C_p

Nomdimensional Chordwise Station, x/c

Figure 32 - Comparative Pressure Distributions, $\alpha \approx 12^\circ$, $q_\infty \approx 32$ lb/ft^2

52
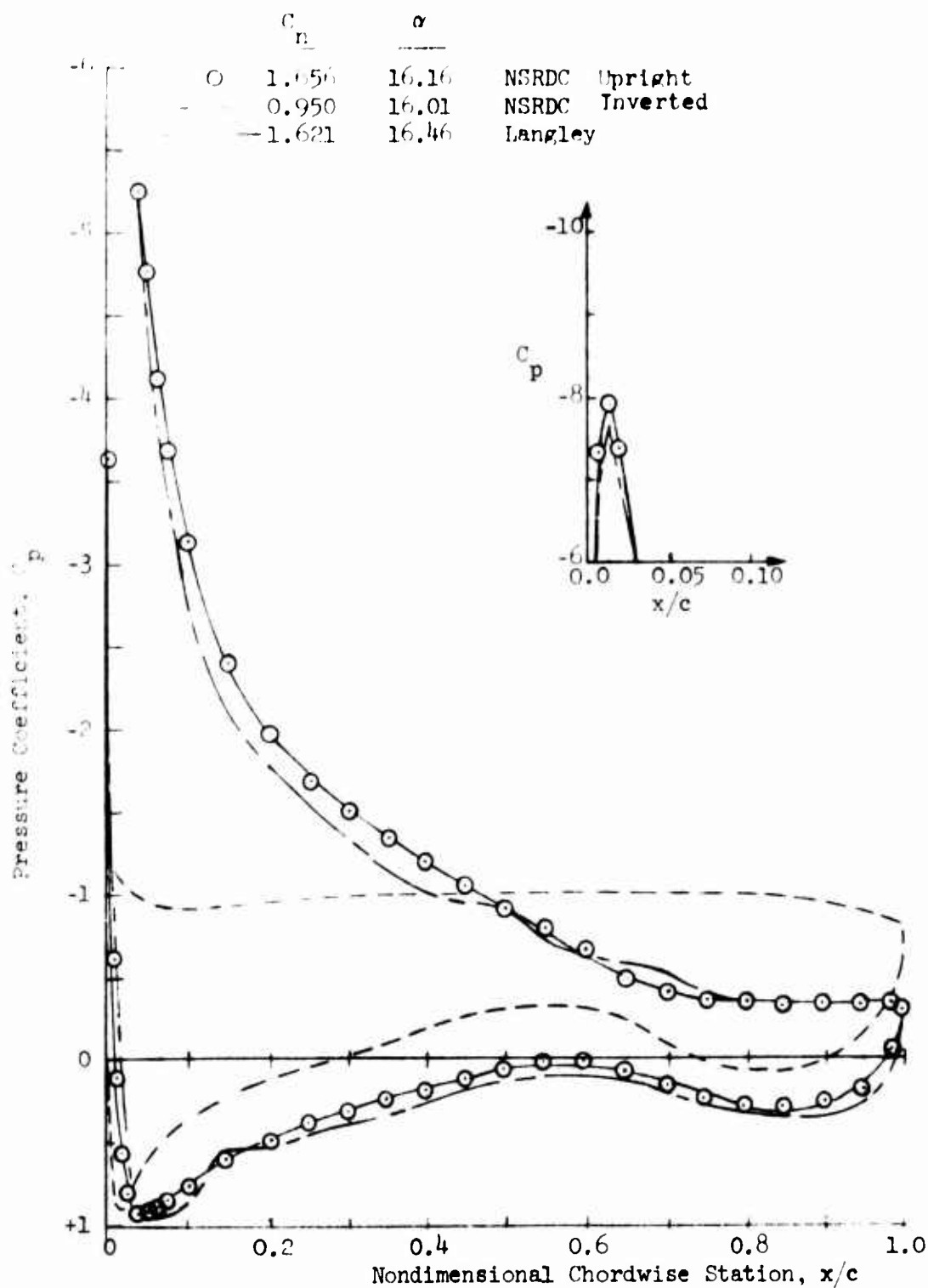
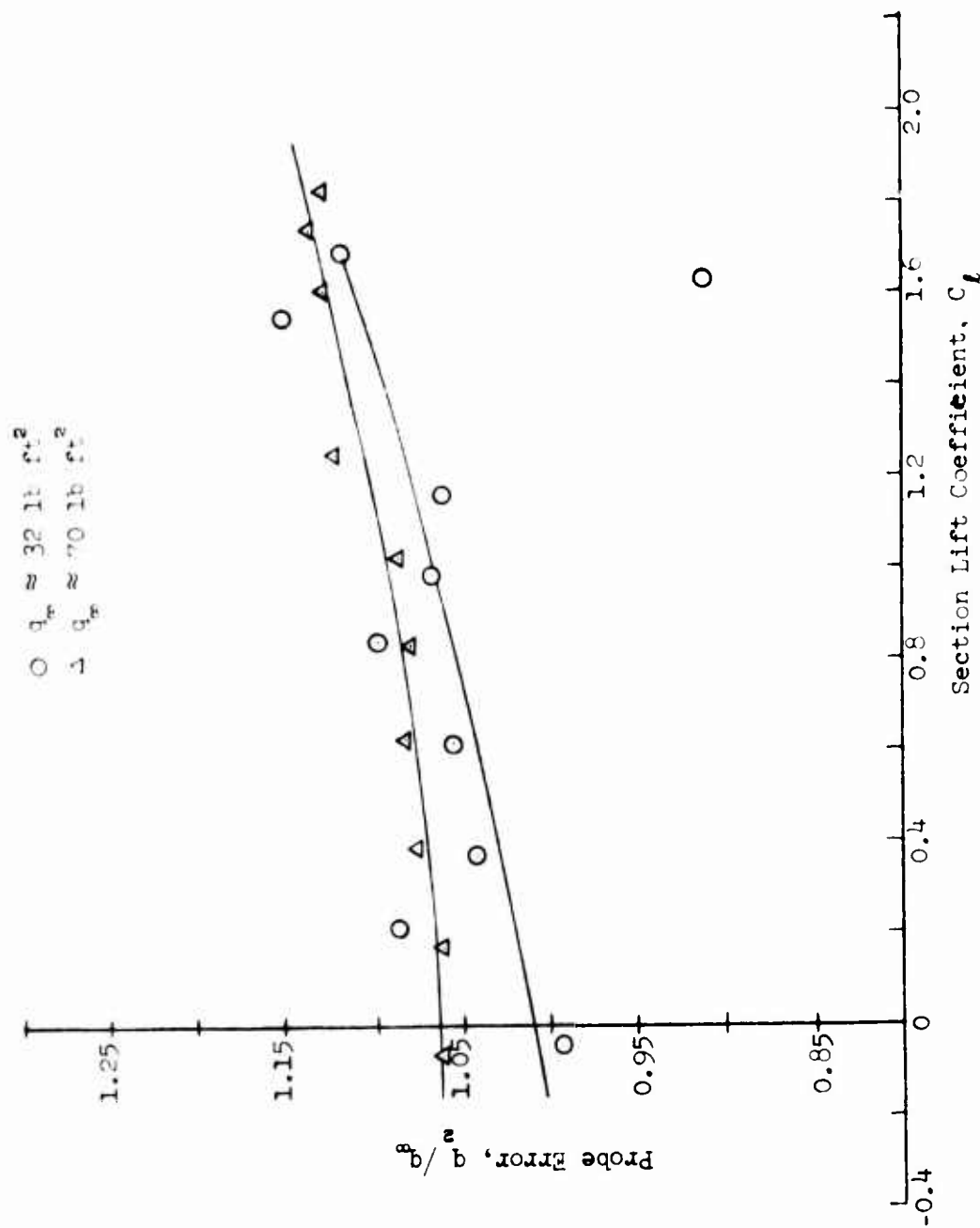Figure 33 - Comparative Pressure Distributions, $\alpha \approx 16°$, $q_\infty \approx 32$ lb/ft²

Figure 34 - Test Section Pitot-Static Probe Error as a Function of Lift and Dynamic Pressure, NASA Reference Section, Upright
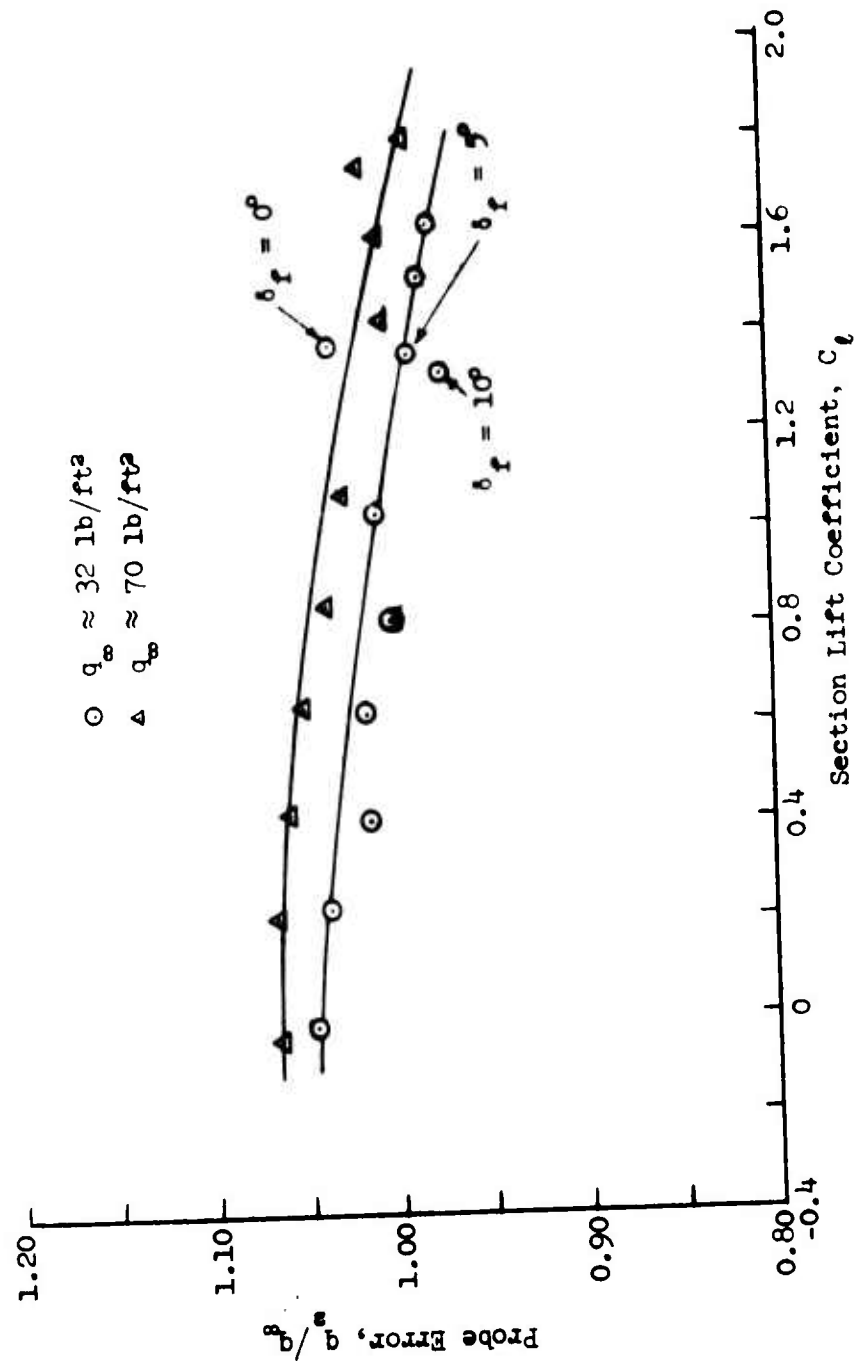
Figure 35 - Test Section Pitot-Static Probe Error as a Function of Lift and Dynamic Pressure, NASA Reference Section, Inverted
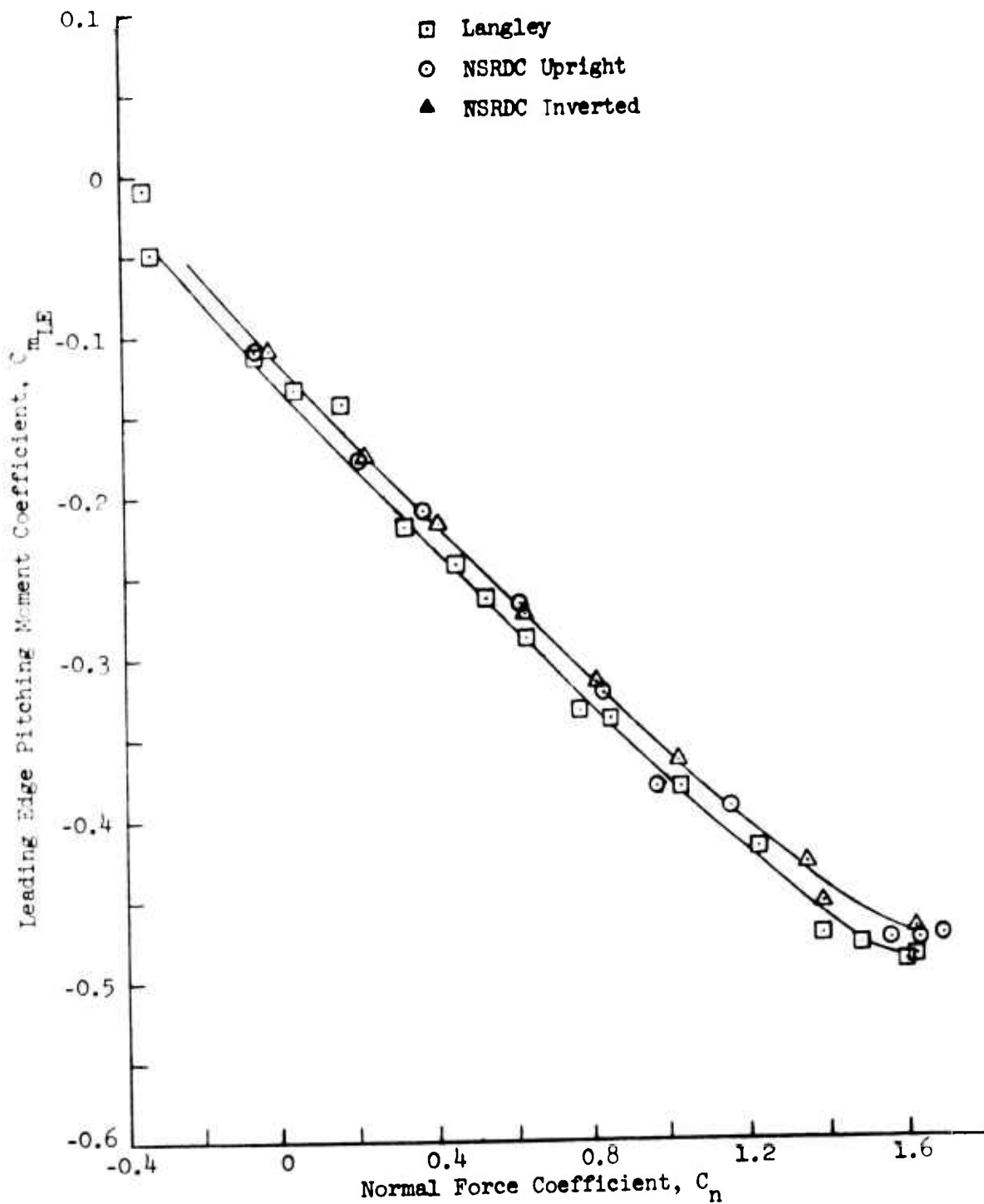
55

Figure 36 - Leading Edge Moment Coefficient for
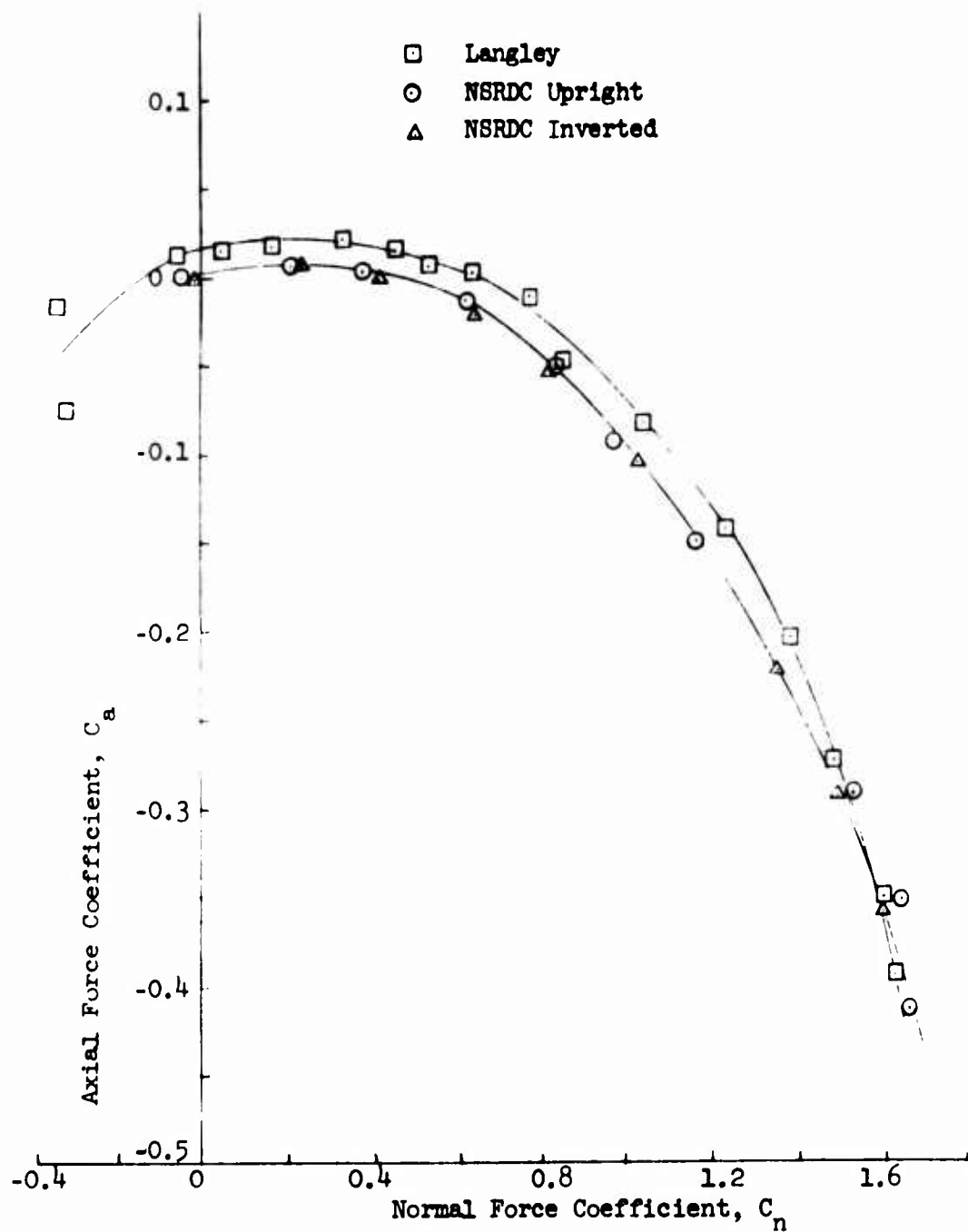NASA Reference Section

56

Figure 37 - Comparative Axial Force Coefficients for
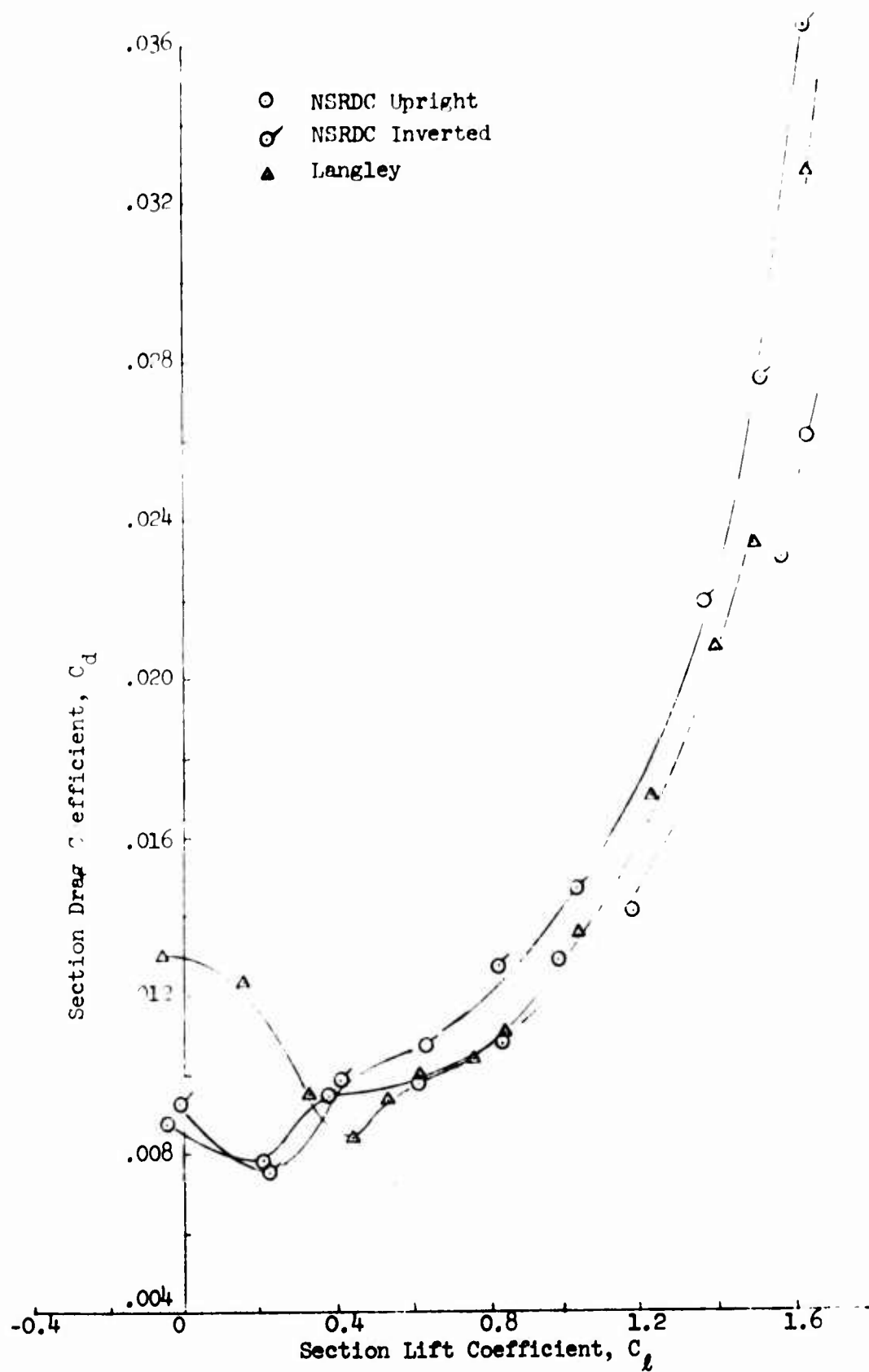the NASA Reference Section

57

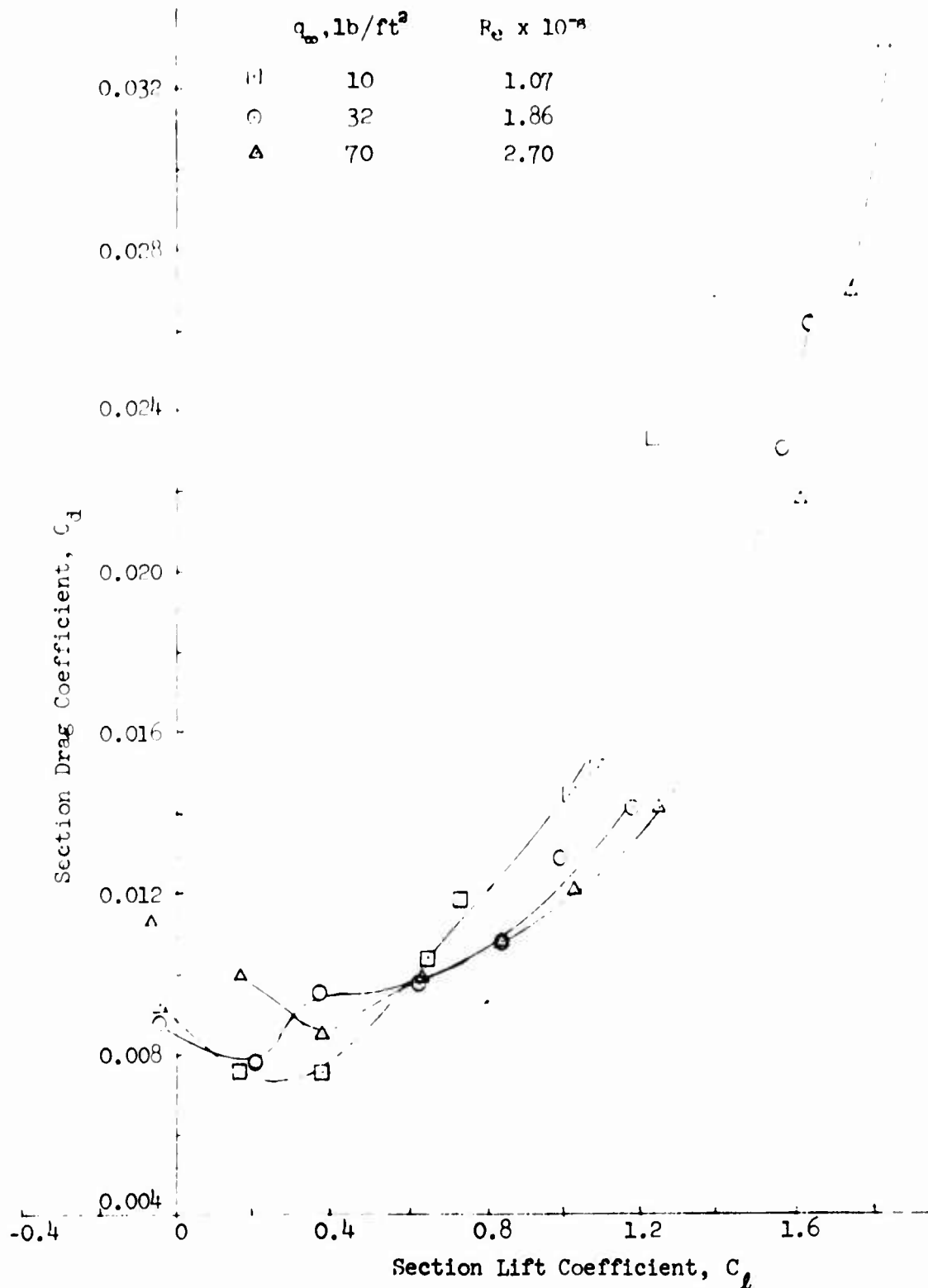Figure 38 - NASA Reference Section Drag Polars, $q_\infty \approx 32 \text{ lb/ft}^2$

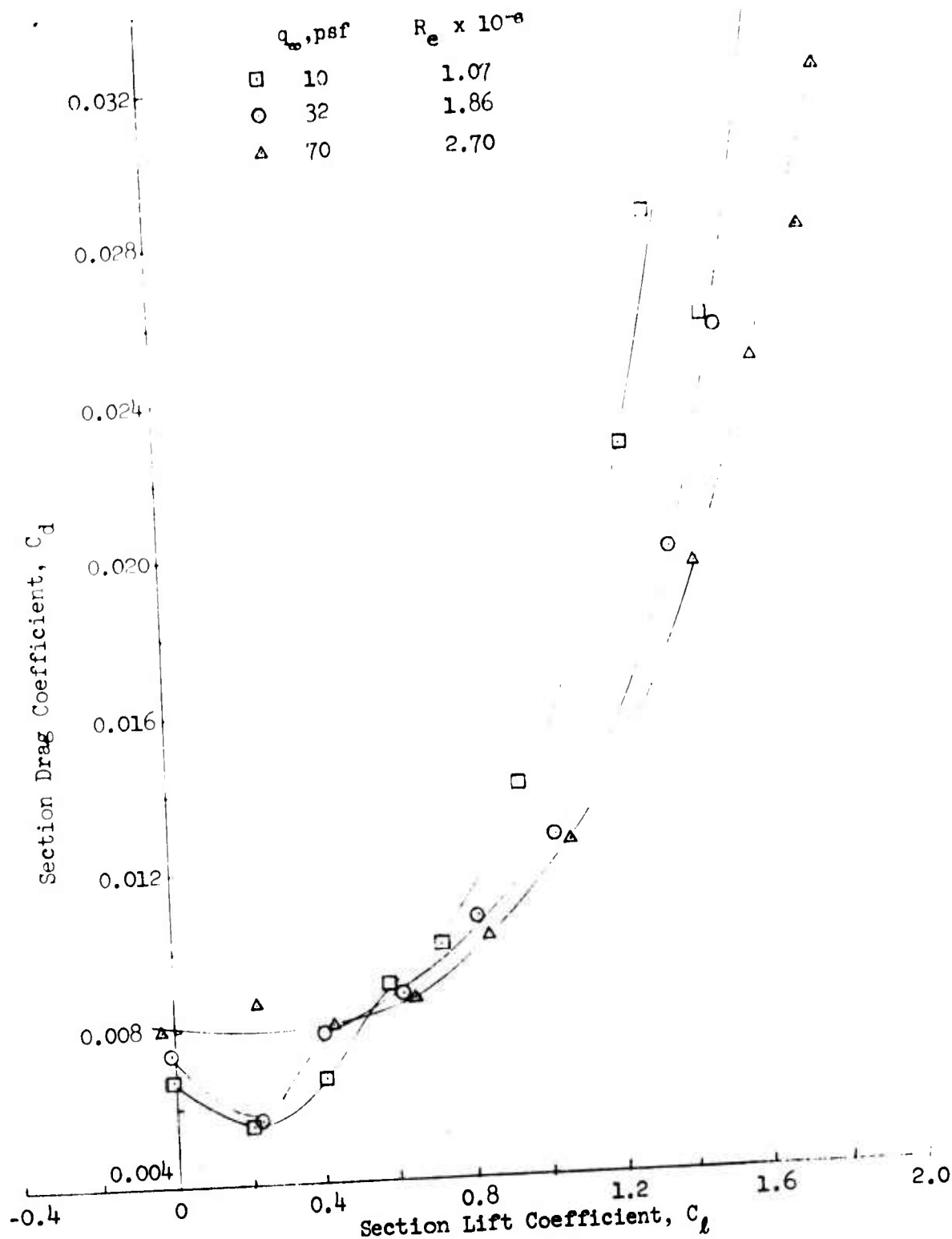Figure 39 - Reynolds Number Effect on Drag Polar, Upright NASA Reference Section

Figure 40 - Reynolds Number Effect on Drag Polar
Inverted NASA Reference Section

Figure 41 - Variation of Wake Rake Total Pressure Distributions with Reynolds Number, Upright NASA Reference Section, $\alpha = 16°$

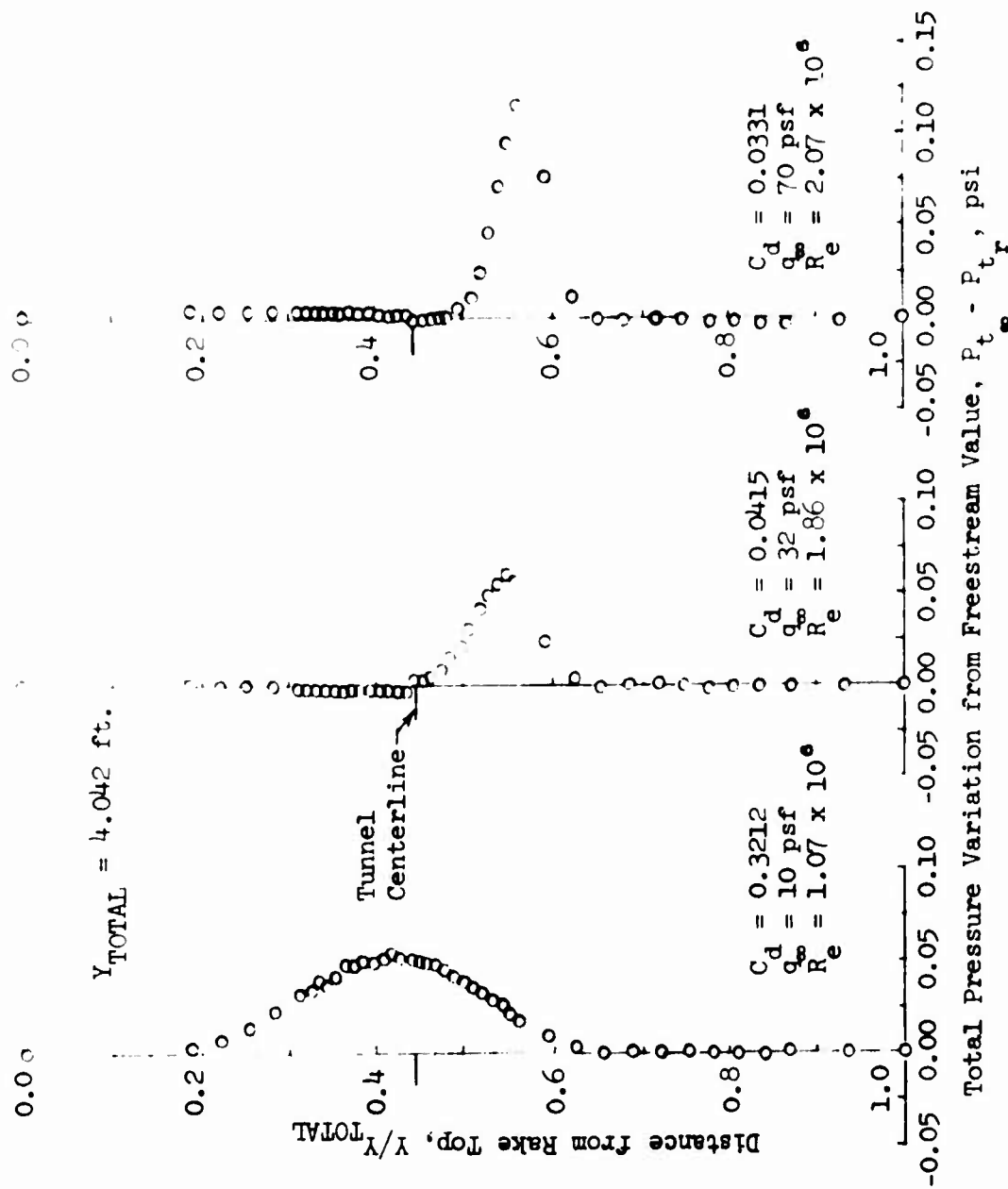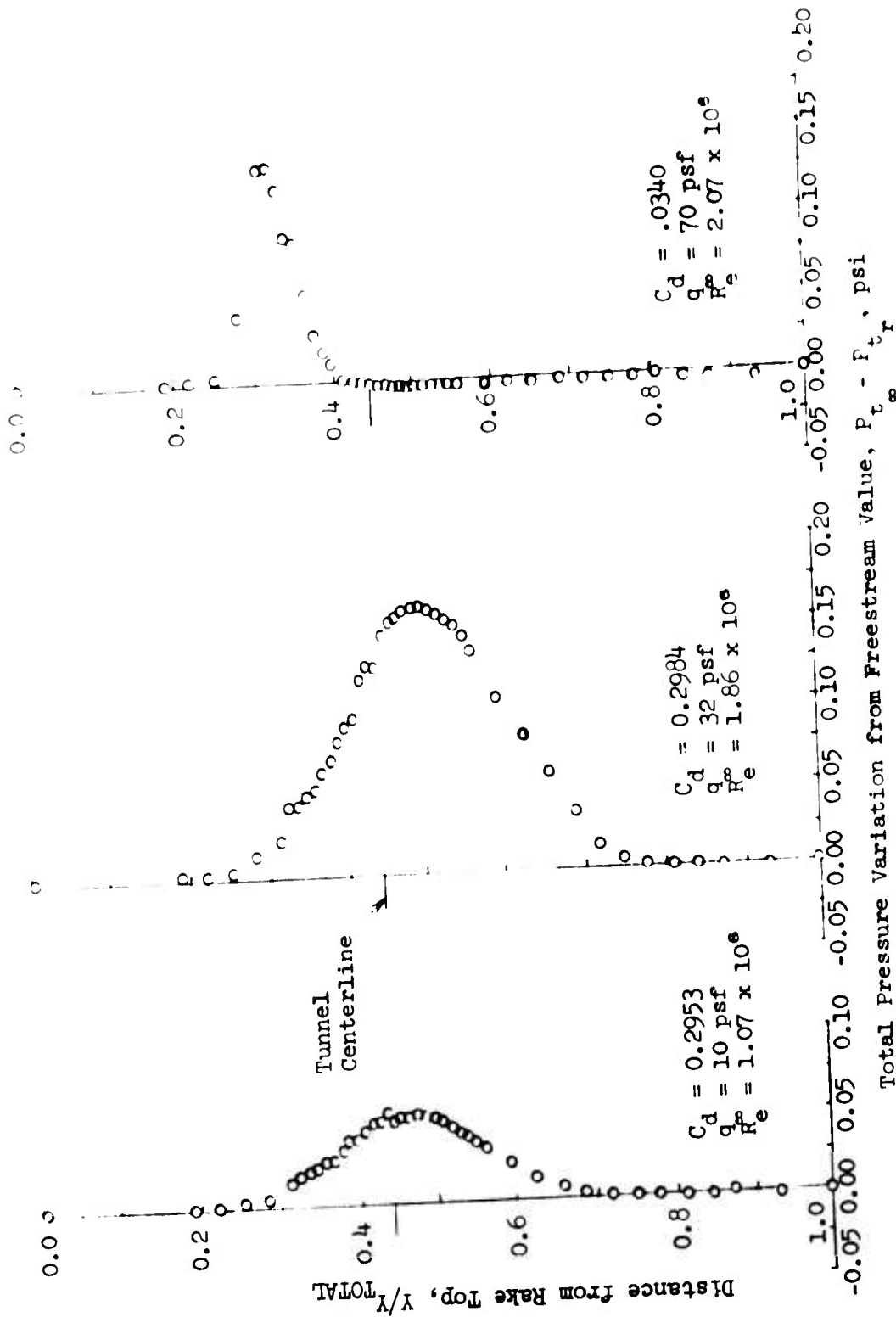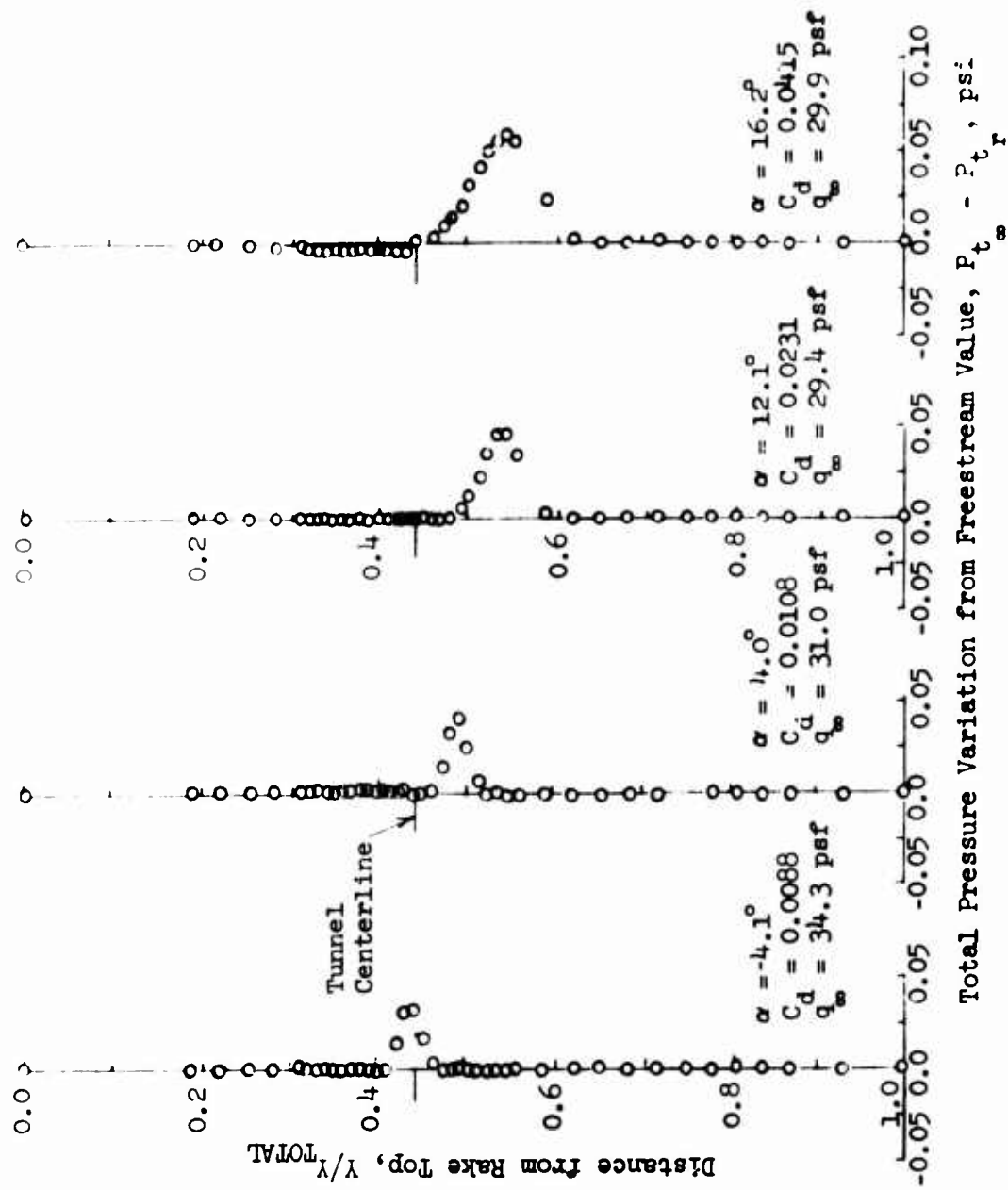Figure 42 - Variation of Wake Rake Total Pressure Distributions with Reynolds Number, Inverted NASA Reference Section, $\alpha = 16$

Figure 43 - Variation in Wake Rake Total Pressure Distribution with Incidence,
Upright NASA Reference Section, $q_\infty \approx 32$ lb/ft²

63

DOCUMENT CONTROL DATA - R & D

(Security classification of title, body of abstract and indexing annotation must be entered when the overall report is classified)

1. ORIGINATING ACTIVITY *(Corporate author)*	2a. REPORT SECURITY CLASSIFICATION
Aviation and Surface Effects Department Naval Ship Research and Development Center Bethesda, Maryland 20034	UNCLASSIFIED
	2b. GROUP

3. REPORT TITLE

CALIBRATION OF THE NSRDC TWO-DIMENSIONAL SUBSONIC PARALLEL WALL WIND TUNNEL INSERTS INCLUDING TESTING OF TWO REFERENCE AIRFOIL SECTIONS

4. DESCRIPTIVE NOTES *(Type of report and inclusive dates)*

Technical Note

5. AUTHOR(S) *(First name, middle initial, last name)*

Robert J. Englar and Jonah Ottensoser

6. REPORT DATE	7a. TOTAL NO. OF PAGES	7b. NO. OF REFS
September 1972	70	7

8a. CONTRACT OR GRANT NO.	9a. ORIGINATOR'S REPORT NUMBER(S)
b. PROJECT NO.	Technical Note AL-275
c. WF 421.212	9b. OTHER REPORT NO(S) *(Any other numbers that may be assigned this report)*
d. NSRDC 690-120	

10. DISTRIBUTION STATEMENT

Distribution limited to U.S. Government agencies only; Test and Evaluation, September 1972. Other requests for this document must be referred to Head, Aviation and Surface Effects Department (16).

11. SUPPLEMENTARY NOTES	12. SPONSORING MILITARY ACTIVITY
	NAVAL MATERIAL COMMAND (03L4) Washington, D.C. 20360

13. ABSTRACT

Parallel wall inserts were installed in the Naval Ship Research and Development Center 8 x 10-foot subsonic tunnel to create a 3 x 8 foot channel to serve as a high flow quality two-dimensional test section for high lift testing. A detailed flow survey indicated good flow uniformity, negligible angularity, a thin wall boundary layer at the model station, and a pronounced effect of trailing edge wall flaps on controlling test section dynamic pressure. A pair of two-dimensional airfoil sections tested in the facility displayed good agreement with reference data in lift and pressure distribution, but some disagreement in wake rake drag data. The strong influence of model lift on test section dynamic pressure measurement was noted, and a measurement technique was developed which was independent of the static pressure field propogating from the airfoil.

14 KEY WORDS	LINK A		LINK B		LINK C	
	ROLE	WT	ROLE	WT	ROLE	WT
Two-Dimensional Wind Tunnel Testing						
High Lift Airfoils						
Parallel Wall Wind Tunnel Inserts						
Two-Dimensional Airfoil Characteristics						
Flow Survey						
Calibration Procedures						
Wall Boundary Layer						
Wall Flaps						